DTNSRDC-ASED-CR-2-83

(12)

AD A125529

EXPERIMENTAL INVESTIGATION OF HIGH PERFORMANCE, SHORT, THRUST AUGMENTING EJECTORS

Tah-teh Yang, Francois Ntone and Jiang Tong
Mechanical Engineering Department
Clemson University
Clemson, SC 29631

January 1983

Prepared for

DAVID W. TAYLOR NAVAL SHIP RESEARCH AND DEVELOPMENT CENTER
Aviation and Surface Effects Department
Bethesda, MD 20084

UNCLASSIFIED

SECURITY CLASSIFICATION OF THIS PAGE (When Data Entered)

REPORT DOCUMENTATION PAGE		READ INSTRUCTIONS BEFORE COMPLETING FORM
1. REPORT NUMBER DTNSRDC-ASED-CR-2-83	2. GOVT ACCESSION NO. AD-A125529	3. RECIPIENT'S CATALOG NUMBER
4. TITLE (and Subtitle) EXPERIMENTAL INVESTIGATION OF HIGH PERFORMANCE, SHORT, THRUST AUGMENTING EJECTORS		5. TYPE OF REPORT & PERIOD COVERED Final Report 6. PERFORMING ORG. REPORT NUMBER CU-ME-F-2-82
7. AUTHOR(s) Tah-teh Yang, Francois Ntone, and Jiang Tong		8. CONTRACT OR GRANT NUMBER(s) DTNSRDC Contract No. N00167-81-C0087
9. PERFORMING ORGANIZATION NAME AND ADDRESS Mechanical Engineering Department Clemson University Clemson, SC 29631		10. PROGRAM ELEMENT, PROJECT, TASK AREA & WORK UNIT NUMBERS
11. CONTROLLING OFFICE NAME AND ADDRESS David W. Taylor Naval Ship R&D Center Aviation and Surface Effects Department Bethesda, MD 20084		12. REPORT DATE January 1983 13. NUMBER OF PAGES 68
14. MONITORING AGENCY NAME & ADDRESS(If different from Controlling Office)		15. SECURITY CLASS. (of this report) UNCLASSIFIED 15a. DECLASSIFICATION/DOWNGRADING SCHEDULE

16. DISTRIBUTION STATEMENT (of this Report)

APPROVED FOR PUBLIC RELEASE: DISTRIBUTION UNLIMITED

17. DISTRIBUTION STATEMENT (of the abstract entered in Block 20, if different from Report)

18. SUPPLEMENTARY NOTES

19. KEY WORDS (Continue on reverse side if necessary and identify by block number)

Contour Wall Diffuser
Ejector
High Performance Ejector
Rotational Flow
Thrust Augmenting Ejector
Reaction Control Ejector

20. ABSTRACT (Continue on reverse side if necessary and identify by block number)

Results of an experimental investigation concerning the design and testing of air-to-air thrust augmenting ejectors utilizing short curved-wall diffusers are presented. These ejectors were designed primarily according to the procedure established in an analytical research effort sponsored by DTNSRDC from 1980-1981. Two of the three ejectors tested have identical mixing chambers. The mixing chamber inlet area to the primary nozzle area ratio λ was 40. The overall ejector

DD FORM 1 JAN 73 1473 EDITION OF 1 NOV 65 IS OBSOLETE
S/N 0102-LF-014-6601

UNCLASSIFIED

SECURITY CLASSIFICATION OF THIS PAGE (When Data Entered)

lambda phi

Block 20 continued AR(diff) L/D(overall)

length-to-mixing chamber diameter ratios ~~(L/D)~~ $_{overall}$ were 6.09 and 6.16; diffuser area ratios $(AR)_{diff}$ were 1.33 and 1.46, respectively. The third ejector had an $(L/D)_{overall}$ of 6.02, a λ of 20 and an $(AR)_{diff}$ of 1.26.

The best observed thrust augmentation ratio ϕ and the modified thrust augmentation ratio ϕ_2 were 2.11 and 1.91 respectively for a sonic primary jet. The modified thrust augmentation ratio ϕ_2 accounts for the penalty of suction in preventing flow separation in the diffuser. These levels of thrust ratio were derived from velocity measurements at the ejector exit. Independent thrust measurements obtained with strain gages on the mixing chamber agree with the force calculated from the momentum data. The experimentally observed ejector performance data correlate well with the predicted values.

phi sub 2

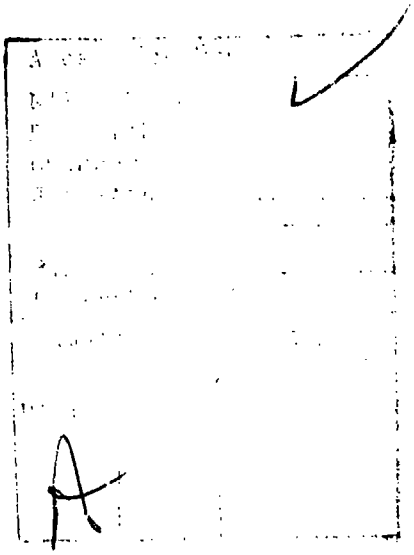

TABLE OF CONTENTS

LIST OF FIGURES

LIST OF TABLES

NOMENCLATURE

f.s.	Ratio of slot suction to total flow rate
$\dot{m}$	Mass flow rate
P	Pressure
V	Velocity
AR	Area ratio
F	Force
L/D	Mixing chamber length to chamber ratio
λ	Mixing chamber inlet to nuzzle area ratio
ϕ	Thrust augmentation ratio
ϕ_2	Modified thrust augmentation ratio
ω	Vorticity

Subscripts

amb	Ambient condition
aux	Auxiliary ejector
e	Exit of diffuser
i	Inlet of diffuser
max	Maximum
mc	Mixing chamber
o	Stagnation condition
p	Primary flow, primary ejector
p'	Primary flow, auxiliary ejector
suc	Suction
Sl	Secondary entrained flow at inlet

EXPERIMENTAL INVESTIGATION OF HIGH PERFORMANCE, SHORT, THRUST AUGMENTING EJECTORS

Tah-teh Yang, Francois Ntone, and Jiang Tong
Mechanical Engineering Department, Clemson University
Clemson, South Carolina

ABSTRACT

Results of an experimental investigation concerning the design and testing of air-to-air thrust augmenting ejectors utilizing short curved-wall diffusers are presented. These ejectors were designed primarily according to the procedure established in an analytical research effort sponsored by DTNSRDC from 1980-1981. Two of the three ejectors tested have identical mixing chambers. The mixing chamber inlet area to the primary nozzle area ratio λ was 40. The overall ejector length-to-mixing chamber diameter ratios $(L/D)_{overall}$ were 6.09 and 6.16; diffuser area ratios $(AR)_{diff}$ were 1.33 and 1.46, respectively. The third ejector had an $(L/D)_{overall}$ of 6.02, a λ of 20 and an $(AR)_{diff}$ of 1.26.

The best observed thrust augmentation ratio ϕ and the modified thrust augmentation ratio ϕ_2 were 2.11 and 1.91 respectively for a sonic primary jet. The modified thrust augmentation ratio ϕ_2 accounts for the penalty of suction in preventing flow separation in the diffuser. These levels of thrust ratio were derived from velocity measurements at the ejector exit. Independent thrust measurements obtained with strain gages on the mixing chamber agree with the force calculated from the momentum data. The experimentally observed ejector performance data correlate well with the predicted values.

ADMINISTRATIVE INFORMATION

This experimental investigation was supported by the David W. Taylor Naval Ship Research and Development Center (DTNSRDC) and the Naval Air Systems Command (NAVAIR) under Navy contract N00167-81-C-0087. The work was technically under the cognizance of D. C. Kirkpatrick (NAVAIR-311D) and T. C. Tai (DTNSRDC 1606).

INTRODUCTION

Background

The use of a jet ejector for augmenting thrust offers a solution to some critical problem areas in the design of vertical/short takeoff and landing (V/STOL) propulsion systems. The benefit of using ejectors, however, is seriously offset by the complexities. The criteria for using such a thrust system are: (1) The system must be short enough to satisfy space and limitations, and (2) it must provide high thrust augmentation to yield a substantial net gain in a practical application.

In 1972 an exploratory experiment was conducted by Yang and El-Nasher[1*] at Clemson University to examine the impact of a highly effective, short diffuser on the flow entrainment of an ejector. Two ejectors were used in that preliminary study. Geometrically, the overall length-to-diameter ratios $(L/D)_{overall}$ of the tested ejectors were 4.9 and 6.5, and both had a contraction at the mixing chamber exit (the diffuser inlet). Steam was used as the primary flow; ambient air was the entrained secondary flow. The necessary boundary layer control for the short diffuser was accomplished with a centrifugal pump. No data were taken to determine the boundary layer suction flow rate and the power consumption of the suction pump. The pressure readings and velocity traverses, however, provided enough information to determine the mass ratios. The mass ratios of these ejectors were several times higher than those of conventional ejectors. Based on the conventional definition of ϕ, the thrust augmentation ratio (not strictly applicable for these ejectors) was calculated from the pressure and velocity measurements. A surprisingly high maximum ϕ value of 2.81 was obtained.

In 1973 a set of experiments was conducted at Clemson by Tripathi[2] to repeat the experiments of Yang and El-Nasher.[1] The previously obtained mass ratio data were confirmed. These ejector experiments, however, did not go much beyond duplication of the 1972 experiments.

A reduction in ϕ value should be expected when air is used as the primary flow instead of steam. A further reduction should be expected in a properly defined thrust augmentation ratio to account for the energy required in boundary layer suction. Nevertheless, the compactness of the ejector and high expected values of the augmentation ratio present an attractive design alternative.

---

*A complete listing of references is given on page 61.

Recent Results

An analytical study was conducted in 1980 under a research contract with DTNSRDC[3] to establish:

1. A method to verify the observed ejector data reported in Reference 1, particularly the high mass ratio.

2. A design procedure for short effective ejectors by incorporating the short, curved-wall diffusers with the ejector mixing chamber design developed by Tai[4] at DTNSRDC. In this analytical investigation, an auxiliary ejector was used to provide the necessary boundary layer control instead of a pump for suction; therefore a self contained, compact ejector was modeled.

Based on the analytical results of Yang and Ntone,[3] the mass ratios derived from the 1972 experimental data are obtainable. Furthermore, an air-to-air ejector with an $(L/D)_{overall}$ of less than 5, which provides an effective augmentation ratio ϕ_2 above 2.0, appears feasible. The effective augmentation ratio is defined in such a way that the inlet momentum of the primary air used in the auxiliary ejector as well as the thrust contribution of the auxiliary ejector are properly taken into account. This level of thrust augmentation ratio can be reached provided the mass ratio of the primary and auxiliary ejectors can be maintained suitably high and the boundary layer suction flow requirement can be held suitably low.

The overall length-to-diameter ratio of the ejector is determined implicitly through use of the required mass flow ratio of the primary ejector to mixing chamber flow. Use of a Griffith-type, short, curved-wall diffuser,[5] coupled with the DTNSRDC design program, offers a significant improvement in $(L/D)_{overall}$ over that obtained with the conventional diffuser. A reduction in $(L/D)_{overall}$ of 30 to 50 percent appears to be feasible.

Objective

The purpose of the present work is to examine experimentally the validity of the ejector design procedure proposed by Yang and Ntone[3] and the values of thrust augmentation ratio of ejectors using short, curved-wall diffusers with mixing chamber inlet area to primary nozzle area ratios of 20 and 40.

EJECTOR DESIGN

An analytical procedure was developed to predict the thrust augmentation ratio of an ejector utilizing a short, curved-wall diffuser.[3] This procedure enabled the pressure distribution to be examined along the solid wall of the diffuser, thus allowing the design of a short, curved-wall diffuser with no flow separation. By this procedure, the predicted ejector performance could be obatined.

Figure 1 shows the major steps in analyzing an axisymmetrical ejector with a short, curved-wall diffuser. The mixing chamber is shaped like a circular pipe which may have a contraction toward the end of the mixing chamber. To initiate the analysis, the area ratio of the primary nozzle to the mixing chamber inlet and the ratio of the mixing chamber length to its diameter (L/D) are specified. The diffuser length usually is restricted to about one exit diameter of the diffuser. In additon, the static pressure at the mixing chamber inlet and stagnation pressure of the primary air are also specified. Both the entrained secondary flow from the stagnant ambient and the primary flow within the nozzle are isentropic up to the mixing chamber inlet. Specifying the static pressure at the mixing chamber inlet, in fact, implies specifying the ratio of the secondary mass flow to the primary mass flow. Starting from the inlet, heat and momentum transfers were allowed between the primary flow and the entrained secondary flow.

The first step in the analysis is to specify the mixing chamber geometry by a selected dimensional value of C in the radius distribution equation of Figure 1 along with other mixing chamber geometric parameters. In step two, the DTNSRDC ejector program[4] is used to compute velocity and temperature profiles and pressure values up to the exit of the mixing chamber. Governing equations for the flow are of the boundary layer type; therefore, pressure variations only exist along the flow directions and not across the streamlines.

In the third step, the mass-averaged flow velocity and temperature are computed. In the fourth step, one-dimensional, compressible isentropic flow is assumed in determining the necessary area ratio to yield the diffuser exit pressure at the atmospheric level (or the ambient level). For other computations in this step, inviscid incompressible axisymmetric

flow is assumed within the diffuser. As long as the flow along the solid wall is maintained without deceleration, the inviscid flow approximation can be justified. Under the framework of this approximation the vorticity of the flow is assumed constant everywhere in the diffuser. The Clemson Inverse Design Program[6] is used to obtain the geometry of the short, curved-wall diffuser for a specified area ratio at a length approximately equal to one exit diameter. This length specification is somewhat arbitrary, yet experience suggests that it should not be difficult to achieve.

Immediately after the determination of the diffuser geometry, a computer program is used in step 4 to examine the velocity distribution along the diffuser wall. It is essential that there be no deceleration along the solid diffuser wall. When necessary, the input for the Inverse Design Program is revised to generate a new diffuser geometry. This process is repeated until there is no deceleration along the diffuser wall. It is sometimes necessary to revise the analysis from the very first step where the mixing chamber inlet pressure is specified. An increase of the static pressure at the inlet implies a reduction in mass ratio and, therefore, a reduction in diffuser area ratio. Usually, this revision can eliminate the problem of deceleration along the solid wall. For a configuration with no deceleration, no flow separation will take place. It is recommended that the velocity from the diffuser inlet to the suction slot be kept slightly accelerated.

The fifth step is to estimate the amount of fluid to be removed for boundary layer control. For this purpose, it is necessary to know the boundary layer profile immediately upstream of the suction slot. It is reasonable to assume that this profile is the same as that at the exit of the mixing chamber. By using this profile, the critical velocity determined by Taylor's criterion can be calculated, and the rate of boundary layer removal can then be determined.

In step 6, the modified thrust augmentation ratio ϕ_2 is computed. The consideration of the mass flow of the primary fluid used in the auxiliary ejectors which provide the necessary boundary layer control and the thrust contribution from the discharge of the boundary layer removal are included in the definition of ϕ_2. A one-dimensional compressible flow analysis, which assumes the mass ratios of the primary and auxiliary ejectors and computes the mass averaged velocity at various parts of the ejector and the momentum terms at the ejector exit, yields the thrust augmentation ratio ϕ_2.

In step 3, the velocity across the mixing chamber exit has been computed, and in step 4 an inviscid shear flow with constant vorticity within the diffuser has been approximated. Therefore, the velocity across the diffuser exit can be readily determined. The last step, Step 7, is to correct the ϕ_2 value by using the known velocity distribution across the diffuser exit.

In the present study, an ejector was first fabricated based on the design using the approximation of constant vorticity in the diffuser for "rotational flow calculation." It was found that this ejector could not be operated without flow separation. A refined analytical procedure which requires no constant vorticity approximation was subsequently devised. Results of the refined analysis indicate that the flow reversal within the first ejector was inevitable regardless of the amount of flow removal for boundary layer control. This flow reversal phenomenon, "inviscid flow reversal," is a consequence of the continuity equation and the vorticity equation requirements. The allowable area ratio of the diffuser without flow reversal obtained using refined analytical procedures is much smaller than that resulting from a constant vorticity analysis. An outline of the "refined rotational flow calculation" is presented in Appendix A.

SCOPE OF EXPERIMENTAL INVESTIGATION

Three ejectors were designed, fabricated, and tested. The design procedure,[3] was refined to allow the vorticity to vary within the diffuser instead of setting the term $(\omega \cdot \nabla)u = 0$, as was approximated in Reference 3. Ejector performance testing was carried out after the mixing chambers and the auxiliary ejectors were improved. The exit vorticity at the mixing chamber, or the inlet vorticity at the diffuser, was measured for each ejector and compared with the analytical predictions. The ducting arrangement of the auxiliary ejector and the nozzle size of the auxiliary ejectors were optimized. A single-jet, converging nozzle having a diameter of 0.448 in. was used as the primary jet for tests at five nozzle plenum pressure levels with four or five boundary layer suction rates. An eight-jet converging nozzle of the same area was used to repeat more than one-half of the test runs of the single jet nozzle. These tests were performed to determine experimentally:

1. Mass ratio MR of the entrained secondary flow to the primary flow of the ejector.
2. Mass ratio $(MR)_{aux}$ of the auxiliary ejector.
3. Thrust of the mixing chamber.
4. Momentum of the flow at the exits of the ejector and the auxiliary ejector.
5. $(\phi_2)_{max}$ as a function of the primary nozzle plenum chamber pressure at various levels of boundary layer removal.

TEST MODELS, FACILITIES, AND MEASUREMENTS

Ejector Geometry

Figure 2 shows the geometry of the first ejector designed without the benefit of the "refined rotational flow calculation" analysis. It has a λ value of 40, a mixing chamber (L/D) of 4.0, and a diffuser area ratio of 2.2. The modified thrust augmentation ratio ϕ_2 was projected to be 1.50. This ejector did not operate satisfactorily. In particular, there was difficulty in getting a reliable mass balance because of flow separation in the diffuser.

Figure 3 shows an ejector which has a λ value of 40, a mixing chamber of 4.82 (L/D), and a diffuser area ratio of 1.33. The diffuser of this ejector can be changed to an area ratio of 1.46 by changing the curved-wall inserts to thus form a new ejector but with the same mixing chamber and λ value.

An ejector with a λ value of 20, a mixing chamber length-to-diameter ratio of 4.75, and a diffuser area ratio of 1.26 is shown as Figure 4. Systematical tests were conducted to determine the effective thrust augmentation ratio ϕ_2 for these three ejectors (diffuser area ratios 1.26, 1.33 and 1.46). Two types of primary nozzles, single-jet and multiple-jet, were used. They are shown in Figures 5 and 6, respectively.

For auxiliary ejectors, a multiple-nozzle (16) annular auxiliary ejector was used on the first ejector having a diffuser area ratio of 2.2; see Figure 7. Although this design concept was discontinued because initial experimental results were unfavorable, it continues to be an attractive design for its compactness and is worthy of further study.

Figure 8 shows the auxiliary ejector used in the ejector performance testing. The ejector is of a conventional design, and the primary nozzle size was optimized for the operational conditions of the main ejectors.

Test Facility

Figure 9 is a schematic of the test setup. Figure 10 shows the ejector performance test setup. The compressed air used as the primary fluid for the ejector and for the auxiliary ejector was supplied by an oil-less ESH Ingersoll-Rand compressor, which has a maximum capacity of 204 ACFM at 90 psig. The compressed air was cooled using an aftercooler and then routed to a 3-ft-diameter 8-ft-high surge tank. From there the air was delivered through a 2-in. pipeline to the laboratory. A gate valve was used to control the air flow into the test loop. A Fisher model 95L (10-30 psig) or model 95H (25-75 psig) regulator was used to regulate the pressure of the primary flow for the ejector nozzle. A Cox turbine flowmeter was installed downstream of the pressure regulator, and an electrical resistance heater (rated 5.6 kW and controlled by a voltage regulator) was placed downstream of the flowmeter. A flexible metal hose was used to connect the heater and the converging nozzle plenum. In the other branch of the test loop, compressed air was supplied to a converging nozzle of the auxiliary ejector. A Norgren model R-17-800 regulator was used upstream of a Meriam laminar flow element. The latter was used to meter the primary flow rate of the auxiliary ejector.

The primary nozzle and the mixing chamber of the test ejector were mounted on an alignment device to ensure that the centerlines of the primary nozzle and mixing chamber were exactly aligned. A set of eight sliding ball bearings were used to allow the mixing chamber to move freely in the axial direction. A force measuring device, utilizing a set of strain gages, was mounted rigidly on the mixing chamber to provide a direct measurement of the thrust force on the mixing chamber. The mixing chamber and the diffuser were assembled together as one integral part which moves freely relative to the alignment rig. The alignment rig was mounted firmly on a stationary supporting stand. The curved wall diffuser insert

downstream of the suction slot could be adjusted relative to the upstream insert to vary the slot size or the gap between the inserts. Four suction ports were provided, and a featherweight flexible hose was used to construct the manifold which led to the inlet of the auxiliary ejector. The primary jet, the mixing chamber, and the diffuser of the auxiliary ejector were all firmly mounted to the stationary stand. The featherweight flexible hose minimized errors in the thrust force measurement on the mixing chamber of the ejector.

Instrumentation and Measurements

Instruments were used in the test for pressure, momentum, mass flow rates, and force measurements at various locations of the loop. First the ambient temperature and pressure were measured using a mercury thermometer and a mercury well-type barometer, respectively. Temperature measurements were made with iron-constant thermocouples, a multi-point selector model 405A and a digital readout Trendicator, both by Omega Instrument Company. The following were used to provide pressure data: one 90-in. U-tube, mercury manometer; one 10-tube, 60-in. mercury manometer bank; one 20-tube, 60-in. water manometer; one Edcliff model 4-500 differential pressure transducer having a range of 0-1 psid; and one Validyne model D-7-D differential pressure transducer with carrier demodulator model CD10 for a range of 0-10 psid along with a 48-channel scanning-valve device. The output of the transducers was displayed on a digital voltmeter manufactured by Nationwide Electronic Systems Inc. Concurrently, the output signal was fed through a laboratory fabricated signal conditioner to a Western Union Data Service Co. teletype which provided a hard copy for the pressure data and a coded paper tape for subsequent computer data reduction. The mass flow rates of the primary flow of the ejector were measured upstream of the converging nozzle using a Cox turbine meter, model AN GL32, and a Hewlett-Packard 5326B counter.

Mass flow rates at the nozzle were determined from local plenum chamber pressure and temperature measurements. The mass flow rates of the primary flow for the auxiliary ejector were measured upstream by using a Meriam laminar flow element and the plenum pressure and temperature measurements. A United Sensor Kiel-probe and a miniature Kiel-probe of the same make were used to determine the mass flow rates at the exits of the

ejector and the auxiliary ejector, respectively. Each of the Kiel-probes was connected to a channel of the scanning valve. Each probe has a holder mounted on a transverse bar with a custom made scale for each tested ejector and auxiliary ejector for rapid 10-point traversing across the exit.

The static pressure of the ejectors was also traversed by using a United Sensor pitot-static probe. A similar probe holder and traversing scale was provided for this also. These traverses provided both mass flow rate and the momentum fluxes at the exits of the ejector and the auxiliary ejector. Indirect measurements of entrained secondary mass flow rates were obtained by traversing at the exit of the mixing chamber of the ejector during the components testing. During several test runs mass flow rates were determined by two independent data sources for verification. In the earlier part of the project, Micro-measurements type EA-13-124AC strain gages were used as sensors and a SR-4 strain indicator type N manufactured by Baldwin Lima Hamilton Company was used for readout of the thrust force on the mixing chamber. Later, an indicator of higher resolution (VISHAY/ELLIS-20) became available and was used for the $\lambda = 20$ single-jet test series. The thrust force measurement provided an independent data source to check the value of exit momentum derived from the Kiel-probe measurements.

TEST CONDITIONS AND PROCEDURE

Test Conditions

After much effort in the preliminary test runs, three ejectors (two with λ equal to 40 and diffuser area ratios of 1.46 and 1.33 and one with λ equal to 20 and a diffuser area ratio of 1.26) were successfully operated without flow separation in their diffuser sections. These ejectors were systematically tested. Table 1 lists the test parameters and performance characteristics for these ejectors. The plenum pressure of each ejector was set at five levels (10, 17.4, 23.2, 29.0, and 35.5 psig, 10 psig being the design value). The ambient static and also the stagnation pressure was approximately 14.5 psia which resulted in pressure ratios of the stagnation pressures of 1.67, 2.21, 2.61, 3.02, and 3.47. The plenum pressure of the primary flow of the auxiliary ejector was selected at five levels (7.5, 10,

12.5, 15, and 17.5 psig) for ejector primary flow plenum pressures of 10, 17.4, and 23.2 psig. The auxiliary plenum pressure was selected at four levels (12.5, 15, 17.5, and 20 psig) at primary flow plenum pressures of 29.0 and 35.5 psig. The temperature of the primary air of the ejector was elevated to 164°F by passing the air through a 6-in. pipe containing suspended electrical heating elements. The heated air expanded through a converging nozzle to reach a static temperature of about 80°F, or approximately the static temperature of the entrained secondary fluid.

The gap between the two curved-wall sections of the diffuser was adjusted to yield a maximum vacuum of the first mixing chamber static pressure reading. Although no exact size was recorded, the gap was between 1/4 and 3/16 in. for all ejectors tested.

Test Procedures

Ejector component test rigs (Figures 11 and 12) were designed to obtain flow velocity profiles at the mixing chamber exit and to obtain the performance of the auxiliary ejector. These rigs were operated at a simulated diffuser condition with no flow separation in the diffuser. In the early stage of the project, the first ejector having λ equal to 40 (using an approximated rotational flow analysis) had a diffuser area ratio of 2.20. This area ratio was too large for the diffuser inlet vorticity, and flow separation persisted in the diffuser. With the refined rotational flow analysis, a new ejector was designed to have an area ratio of 1.64; this area ratio was still too large. The computed vorticity obtained from the DTNSRDC computer program used in the rotational flow analysis was lower than the value derived from the measured velocity at low pressure ratios of the stagnation pressures. Until the diffuser area ratio was reduced to 1.46, flow separation within the diffuser persisted. Considerable effort was required to eliminate flow separation in the short, curved-wall diffuser, and this was achieved largely on the ejector performance test stand rather by component testing.

The mixing chamber length for a λ of 40 was also reduced from 15.5 to 13.5 in. on the ejector performance test stand. The first mixing chamber wall static pressure tap was used to monitor the flow rate of the entrained secondary flow, and tufts attached at the diffuser exit were used as indicators for flow attachment. In this length reduction process, no

secondary flow reduction was detected in the first one inch trimming. A reduction of 0.2 in water was observed in the wall static pressure reading when the length was reduced to 13.5 in. No flow separation was indicated by the tufts. This process was carried out at a plenum pressure of 10 psig for the primary flow of the ejector.

The preliminary test for the auxiliary ejector went through several design concepts. First, a 16-nozzle annular ejector with only the mixing chamber was tested. An annular diffuser was later added to the exit of the mixing chamber. Three sets of nozzle lengths were used to regulate the nozzle exit position relative to the entrained flow inlet. The annular auxiliary ejector effort was conducted using an ejector diffuser with an area ratio of 2.20. As satisfactory results were observed, an auxiliary ejector with a cylindrical mixing chamber and a long conical diffuser was used. The exit diameter of the converging nozzle of the cylindrical auxiliary ejector was optimized to yield a maximum mass ratio for the ejector operating at a primary plenum pressure P_o of 10 psig.

When the preliminary tests were completed, systematic test runs commenced. For each test run the plenum pressure levels for the primary and auxiliary ejectors were adjusted to the preselected values via pressure regulators and monitored by manometers. The plenum temperature of the primary air of the main ejector was regulated to yield a preselected temperature by adjusting the voltage regulator of the electrical heater. A miniature Kiel-probe was used to traverse the auxiliary ejector exit. A Kiel-probe and a static pressure probe were used to traverse the main ejector exit. A 10-point method was used for traversing the entire diameter yielding 20 stations for both stagnation and static pressure readings. These pressure readings and the wall pressure readings of the mixing chambers and the diffusers were recorded either via pressure transducer-scanning valve to teletype arrangement or pressure transducer-scanning valve to an Apple computer for data reduction. Strain gage output was read as a direct measurement of the force on the mixing chamber. Normally, 30 to 40 minutes was required to complete one test run. Care was exercised to ensure that the pressure levels of the primary flows, the temperature of the heated air, and the strain gage output readings did not "drift" during the test period. Therefore, these readings were repeated at the end of each test run. The method of data reduction is presented in Appendix B.

DISCUSSION OF RESULTS

The results of this experimental investigation are presented for: (1) the maximum modified thrust augmentation ratio $(\phi_2)_{max}$ versus primary nozzle pressure ratio P_o/P_{amb}; (2) a comparison between the theoretically predicted and the experimentally determined ϕ_2; (3) a comparison between values of thrust force on mixing chamber determined from direct force measurements and those determined from the integrated momentum measurements at the diffuser exit; (4) a typical velocity distribution at the exit of the mixing chamber, computed and measured; (5) a typical velocity distribution at the diffuser exit, computed and measured; and (6) typical wall pressure distributions for the mixing chamber and diffuser.

Thrust Augmentation Ratio versus Primary Nozzle Pressure Ratio

Figure 13 shows the loci of the maximums of ϕ_2 versus the primary nozzle pressure ratio. The number shown in Figure 13 adjacent to the data point refers to the run number listed in Table 1. This curve was derived from a set of parametric performance curves in Figure 14 for $\lambda = 40$, AR = 1.33, $(L/D)_{overall} = 6.09$ and a single jet converging primary nozzle. The first data point in Figure 13 is for $\phi_2 = 1.66$ at a pressure ratio of 1.67, which was the pressure ratio used in the design of the test ejector. The next maximum occurred at a higher value of ϕ_2 when the pressure ratio was increased to 2.21. The peak in ϕ_2 reached 1.88 at the tested pressure ratio of 2.61. Any further increase in pressure ratio resulted in a decrease of ϕ_2.

The Parametric performance curves in Figure 14 show that at low pressure ratio, ϕ_2 increased as the boundary layer suction was increased. Initially, an increase in $P_{o,aux}$ led to an increase of mass entrainment $\dot{m}_{sl}$ and an increase in mass flow rate $\dot{m}_e$ at the ejector exit. The value of $\dot{m}_{sl}$ continued to increase with further increase in suction, but $\dot{m}_e$ decreased. For each primary nozzle plenum pressure P_o, there is a maximum value of momentum at the ejector exit. The change of suction percentage values for peaks of ϕ_2 at different pressure ratio P_o/P_{amb} does not exhibit a simple trend due to the definition of ϕ_2, which reflects not only the performance of the ejector but also that of the auxiliary ejector;

for example, at P_o/P_{amb} = 1.67, $(\phi_2)_{max}$ occurred at 13-percent suction. When P_o/P_{amb} increased to 2.21, however, the $(\phi_2)_{max}$ occurred at 7-percent suction, and at P_o/P_{amb} = 2.61, $(\phi_2)_{max}$ occurred at 5.7-percent suction. Further increase in pressure ratios to values of 3.02 and 3.47 resulted in the shifting of peaks to 6 and 6.5-percent respectively.

Three of the five parametric curves shown in Figure 14 were repeated with an eight-jet converging nozzle; otherwise the test conditions were unchanged. This nozzle has a total exit area of 0.153 in^2, while the single-jet nozzle has an exit area of 0.146 in^2. Although it was intended to have two nozzles with the same exit area, fabrication difficulties caused a slight difference. Figure 15 shows the loci of the peaks of ϕ_2, and Figure 16 shows the parametric performance curves. The curve in Figure 15 is substantially lower than that in Figure 13. Tai[4] has shown potentially that an annular nozzle would have a higher thrust augmentation ratio. The present investigation did not demonstrate this potential. It is believed that blockage of the center passage at the ejector inlet should, in part, account for the deficiency.

Figure 17 shows the loci of $(\phi_2)_{max}$ versus the pressure ratio P_o/P_{amb} for an ejector having λ = 40, AR = 1.46, $(L/D)_{overall}$ of 6.16 and a single-jet nozzle. In fact, the same mixing chamber was used in the ejector as that presented in Figure 13. Curves shown in Figures 14 and 18 are similar. The entrained mass flow $\dot{m}_{sl}$, in general, is slightly higher for the ejector with AR = 1.46 than for the one with AR = 1.33. The peak values of the exit momentum, however, were slightly lower for the former than the latter. The primary flows $\dot{m}_p$ of the auxiliary ejector for both diffusers were approximately the same; while the suction flow rates $\dot{m}_{suc}$ were higher in the unit having AR = 1.33 than in the one with AR = 1.46 because a lower vacuum existed across the suction slot in the diffuser having AR = 1.33. It is apparent that for the same ejector exit momentum, a diffuser with the smallest area ratio should be used. For AR = 1.46, a value of $(\phi_2)_{max}$ equal to 1.91 occurred at a P_o/P_{amb} value of 2.6. The design pressure ratio was 1.67. Figures 19 and 20 are results for an ejector of AR = 1.46, $(L/D)_{overall}$ = 6.16 with an eight-jet primary nozzle. The value of $(\phi_2)_{max}$ = 1.64 occurred at P_o/P_{amb} = 2.6.

Figure 21 shows the loci of $(\phi_2)_{max}$ for each tested pressure ratio P_o/P_{amb} for an ejector of $\lambda = 20$, AR = 1.26, $(L/D)_{overall} = 6.02$ and a single-jet nozzle. This mixing chamber cross-sectional area is onehalf of that of the mixing chamber of the two previously described ejectors. The peak of Figure 21 is 1.50 versus a value of 1.91 for $\lambda = 40$. Over a broad range of pressure ratios, this ejector was able to maintain a value of about 1.50. Figure 22 shows the parametric performance curves from which Figure 21 was derived. Figures 23 and 24 are similar to Figures 21 and 22, except that and eight-jet nozzle was used instead of a single- jet nozzle.

Ejector performance versus pressure ratios for ejectors with AR = 2.0 and $\lambda = 40$ (Reference 3) were computed with assumed values of fraction of suction, f.s., and mass ratio of the auxiliary ejector $(MR)_{aux}$. Using the experimentally measured values of f.s., $(MR)_{aux}$, and vorticity ω at the diffuser inlet and the analytical procedure of Yang and El-Nasher,[1] three performance curves (one for each ejector tested) were obtained. Figure 25 shows these curves of predicted ϕ_2 versus pressure ratio P_o/P_{amb}. The discrete points are experimental data. In essence, this comparison reflects the validity of the global analysis developed by Yang and Ntone[3] and the refined rotational flow analysis developed during the present experimental investigation. Good agreement is observed between the analytically computed and the experimentally observed ϕ_2 values over a major part of the P_o/P_{amb} range.

Thrust Augmentation

The thrust of the type of ejectors studied in this investigation is the integrated force at the ejector exit. As stated, the values of this force were obtained using two approaches: (1) the difference between the momentum at the ejector exit and the momentum at the primary nozzle exit and (2) the direct force measurement using the strain gage arrangement (see section on Instrumentation and Apparatus). Figures 26 through 31 show comparisons of the integrated forces determined from the two different approaches for ejectors with AR = 1.26, AR = 1.33 and AR = 1.46. Again, the number shown in the above figure adjacent to each data point refers to the run number listed in Table 1. A majority of the data points fall on a line of 45 deg., but are displaced up to 0.3 lb to give higher values of

thrust derived from the momentum measurements. It is believed that the experimental apparatus was not totally free to move before the cantilever arm of the mixing chamber came into contact with the motion stop. There appears to be a small but systematical error in the strain gage force measurements introduced by the presence of the suction manifold of the auxiliary ejector. Allowing for this, the thrust determined from the two approaches shows good corelation with most of the data in the low and medium tested pressure ratios of P_o/P_{amb}. Greater deviations were observed in the high pressure range for multi-jet nozzle test runs. This increased deviation could be due to the static pressure across the mixing chamber inlet not being constant as was assumed.

Velocity Distributions

Figure 32 shows two typical normalized velocity distributions. The distribution indicated by the solid line was obtained using the DTNSRDC computer program of Tai.[4] Experimentally measured mass ratio MR and pressure ratio P_o/P_{amb} were used as inputs for this computation. This mixing chamber exit is located 4.82 diameters downstream from its inlet. The velocity distribution shown by discrete points was obtained using a miniature Kiel-probe and a static pressure probe. Basic features of a shear flow were observed in both profiles. Because of the size of the probes, no measurements were taken closer than 1/16 in. from the wall. The vorticity values derived from the measured velocity are about 10 percent higher than those derived from the computed distribution at $P_o/P_{amb} = 1.67$. Good agreement in vorticity values was observed at higher pressure ratios. Fifteen sets of velocity distribution were examined for this investigation. In static pressure measurements the centerline pressure usually was 1.0 to 2.0 in. of water lower than that at the wall.

The velocity measurements at the exit of the mixing chamber provided information for correcting vorticity ω in computing diffuser exit velocity for the rotational flow analysis. The velocity measurements also provided an independent source from which the entrained flow rate $\dot{m}_{sl}$ was determined. Figures 33 and 34 provide similar information for ejectors having AR values of 1.46 and 1.26, respectively.

Figure 35 shows a typical exit velocity distribution for an ejector having AR = 1.33. The solid line curve is the computed velocity distribution using the refined rotational flow analysis; See Appendix A. The feature of shear flow is preserved in both the computed and the experimentally measured velocity distributions. Steady flow prevailed over the entire test ranges of p_o and $p_{o,aux}$.

The velocity measurements at the diffuser exit provided key elements of data for evaluation of thrust augmentation ratio ϕ_2, mass flow rate $\dot{m}_e$, and mass flow ratio MR. The MR is defined as $\dot{m}_{sl}/\dot{m}_p$, and the entrained mass flow rate $\dot{m}_{sl}$ was determined from

$$\dot{m}_{sl} = \dot{m}_e + \dot{m}_{suc} - \dot{m}_p$$

Then,

$$\dot{m}_{suc} = \dot{m}_{e,aux} - \dot{m}_p.$$

Independent checks on $\dot{m}_{sl}$ were made using the equation

$$\dot{m}_{sl} = \dot{m}_{mc} - \dot{m}_p$$

The values of $\dot{m}_{sl}$ as determined from these two independent approaches differed by no more than 4 percent; therefore, the MR values are considered to be accurate within 4 percent.

Figure 36 shows the typical velocity distribution of the ejector having AR = 1.46. In this figure, the measured velocity distribution shows a slight asymmetric nature of the flow. During the test a certain degree of unsteadiness was observed in a small region near the left side of the diffuser wall. Figure 37 shows the similar information for the ejector with AR = 1.26. Steady flow prevailed in this ejector over most of the operating ranges of P_o and $P_{o,aux}$, except when P_o was around 30 psig. In all three figures the measured peak velocities fall below the computed values. During the test, unusual velocity distributions were observed both at the exit of the mixing chamber and at the exit of the diffuser for the ejector with AR = 1.26 and λ = 20 when the primary nozzle plenum pressure was set between a narrow range of 30 to 31 psig. These profiles are presented in Figures 38 and 39.

Wall Pressure Distributions

Figure 40 shows the typical measured and computed pressure distributions along the diffuser wall for an ejector having AR = 1.33. The computed pressure distribution used the computer program of Tai[4] for the mixing chamber portion and the Bernoulli equation in conjunction with the wall velocity from rotational flow analysis for the diffuser portion. The wall pressure readings throughout the ejectors were below ambient pressure. The static pressure at the end of the bell mouth was used as the normalizing factor. The computed pressure level within the mixing chamber was significantly lower than the measured level. Within the diffuser favorable pressure gradients were prescribed initially to the solid wall portion (upstream and downstream of the suction slot) of the diffuser designed with the irrotational flow, inverse design program. The rotational flow computation also predicted favorable pressure gradients. Owing to the fact of low diffuser area ratio, attached flows were maintained even though the experimental data exhibited deceleration both upstream and downstream of the suction slot.

Figures 41 and 42 show the wall pressure distributions for ejectors with AR = 1.46 and 1.26, respectively. In spite of a seemingly over-deceleration exhibited immediately upstream of the suction slot of the ejector with AR = 1.26, no apparent flow separation was observed. The attached flow may be attributed to the low AR value. In Figures 40, 41, and 42, the feature of sudden pressure rise across the suction slot was also preserved in the measured pressure distribution.

CONCLUSIONS AND RECOMMENDATIONS

It is noteworthy that the peak values of the thrust augmentation $(\phi_2)_{max}$ reached 1.91, 1.89 and 1.62 for $\lambda = 40$, $(L/D)_{overall} = 6.16$ and 6.09 and for $\lambda = 20$, $(L/D)_{overall} = 6.02$, respectively. Higher values of $(\phi_2)_{max}$ and shorter overall length-to-diameter ratios are believed to be possible with further improvement of the auxiliary ejector.

The computation and measurements of $(\phi_2)_{max}$ versus P_o/P_{amb} for each of the three ejectors are in good agreement. The differences are attributed to the analytical assumptions that (1) uniform and ambient static pressure prevailed at the ejector inlet, (2) uniform static pressure existed at the diffuser inlet, and (3) the flow was inviscid in these diffusers. The error introduced by the assumptions of uniform and ambient static pressure was more pronounced when the ejectors were operated at higher levels of P_o/P_{amb} ratios, where the entrained velocities were high. The deviations between the measured thrust on the mixing chamber and that calculated from the momentum considerations are larger at higher P_o/P_{amb} levels. Relaxing these analytical assumptions would increase the cost of computation considerably. The estimated maximum possible error in the measured $(\phi_2)_{max}$ is ± 5 percent of the values presented. The predicted pressure distributions along the diffuser wall deviated from the measured values, particularly near the suction slot. Improvement in the rotational flow computation is needed.

It is envisioned that ejectors of the type tested would have potential application to flight controls such as yawing and rolling of V/STOL aircraft. In this application, the overall length of the ejectors perhaps should be further reduced.

During the project, it became apparent that a computer code for an inverse solution of rotational flow to design the diffuser would be highly desirable, particularly to further improve $(\phi_2)_{max}$.

The auxiliary ejector of the test model and the ducting used in this investigation could be designed more compactly. The original concept of using an annular auxiliary ejector was abandoned halfway through the project because of the unsuccessful operation of the diffuser with an area ratio of 2.2. It is highly probable that the annular auxiliary ejector could have worked for a diffuser with an area ratio of 1.33 or 1.26.

Further recommendations are to:

1. Establish a computer code of inverse rotational flow for the diffuser design to simplify the computational procedure and to optimize the ejector momentum output.
2. Refine the auxiliary ejector design to further improve the performance.

TABLE 1 - PARAMETERS AND PERFORMANCE CHARACTERISTICS
OF SINGLE- AND MULTI-JET NOZZLES

AR = 1.33 λ = 40 nozzle SINGLE-JET

run	P_o	P_{aux}	$\dot{m}_p$	$\dot{m}_{p'}$	$\dot{m}_e$	$\dot{m}_{e,aux}$	$\dot{m}_{suc}$	$\dot{m}_{sl}$	$\dot{m}_{mc}$	fs%	MR	$(MR)_{aux}$	$(\dot{m}v)_e$	$(\dot{m}v)_{e,aux}$	$(\dot{m}v)_j$	$(\dot{m}v)_{j,aux}$	$(\frac{\phi-1}{\dot{m}v})_j$	Thrust	ϕ	ϕ_2
	psig		lbm/s										lbm-ft/s^2				lbf			
1	10.0	7.5	.0764	.0132	.6563	.0723	.0590	.6389		8.2	8.36	4.47	134.9	4.1	81.0	11.8	1.67	1.55	1.67	1.50
2	10.0	10.0	.0758	.0144	.6475	.0883	.0740	.6457		10.3	8.52	5.14	133.2	6.0	80.3	13.9	1.65	1.65	1.66	1.48
3	10.0	12.5	.0760	.0161	.6792	.1016	.0854	.6886		11.2	9.06	5.29	144.3	8.1	80.7	16.8	1.98	1.65	1.79	1.56
4	10.0	15.0	.0759	.0176	.6556	.1181	.1005	.6302	.7154	13.3	8.96	5.57	154.3	10.8	80.4	18.3	1.69	1.80	1.91	1.66
5	10.0	17.5	.0761	.0182	.6621	.1220	.1038	.6878		13.5	9.03	5.71	140.1	11.8	81.2	18.9	1.83	1.86	1.73	1.52
6	17.4	7.5	.1000	.0124	.8515	.0667	.0593	.8088		6.0	8.05	4.39	210.0	3.4	111.7	10.8	3.05	2.64	1.88	1.74
7	17.4	10.0	.1000	.0134	.8675	.0795	.0661	.8336	.8998	7.1	8.34	4.93	221.0	4.9	111.8	13.0	3.39	2.74	1.98	1.81
8	17.4	12.5	.1000	.0164	.8747	.0935	.0771	.8518		8.1	8.52	4.70	222.6	6.8	111.7	17.1	3.44	2.79	1.99	1.78
9	17.4	15.0	.1002	.0177	.8722	.1062	.0886	.8491		9.3	8.47	5.01	223.1	8.7	112.3	18.4	3.44	2.83	1.99	1.77
10	17.4	17.5	.0997	.0203	.8659	.1182	.0980	.8642		10.2	8.67	4.83	218.7	8.7	111.8	21.1	3.32	2.88	1.96	1.73
11	23.2	7.5	.1189	.0122	.9458	.0617	.0496	.8765	.9747	5.0	7.37	4.08	262.4	2.9	132.9	10.6	4.02	3.32	1.97	1.85
12	23.2	10.0	.1187	.0141	.9641	.0774	.0583	.9037		5.7	7.61	4.14	271.2	4.0	132.7	13.7	4.30	3.40	2.04	1.88
13	23.2	12.5	.1174	.0164	.9385	.0836	.0671	.8869		6.7	7.55	4.08	257.3	5.4	131.6	17.1	3.90	3.50	1.96	1.77
14	23.2	15.0	.1178	.0180	.9400	.0944	.0764	.8986		7.5	7.63	4.25	257.8	6.9	132.1	18.7	3.91	3.55	1.95	1.76
15	23.2	17.5	.1179	.0182	.9735	.1063	.0881	.9457		8.3	8.0	4.85	256.4	8.8	131.7	19.0	3.95	3.70	1.95	1.76
16																				
17																				
18	29.0	12.5	.1354	.0164	1.0205	.0743	.0579	.9430	1.0766	5.4	6.96	3.53	306.5	4.3	151.5	15.9	4.81	4.25	2.02	1.86
19	29.0	15.0	.1337	.0182	1.0205	.0890	.0708	.9516		6.5	7.16	3.88	301.1	6.2	149.8	19.0	4.89	4.41	2.05	1.86
20	29.0	17.5	.1362	.0199	1.0214	.1024	.0825	.9676		7.5	7.10	4.14	309.0	8.2	152.3	20.7	4.87	4.50	2.03	1.83
21	29.0	20.0	.1362	.0214	.9989	.1139	.0925	.9560		8.5	7.06	4.32	295.5	10.0	151.4	22.3	4.48	4.50	1.95	1.76
22																				
23																				
24	35.5	12.5	.1544	.0164	1.0434	.0746	.0582	.9472	1.1273	5.3	6.13	3.51	335.4	4.3	172.1	17.1	5.11	4.80	1.96	1.80
25	35.5	15.0	.1544	.0180	1.0667	.0922	.0742	.9865		6.5	6.39	4.12	347.0	6.5	172.4	18.7	5.43	4.96	2.01	1.85
26	35.5	17.5	.1544	.0202	1.0568	.1029	.0828	.9852		7.3	6.38	4.10	344.0	8.2	172.8	21.0	5.23	5.03	1.98	1.80
27	35.5	20.0	.1544	.0214	1.0959	.1101	.0887	1.0342		7.5	6.67	4.15	360.2	9.3	172.9	22.3	5.82	5.63	2.08	1.89

TABLE 1 (continued)

AR = 1.33 λ = 40 nozzle EIGHT-JET

run	P_o	P_{aux}	$\dot{m}_p$	$\dot{m}_{p'}$	$\dot{m}_e$	$\dot{m}_{e,aux}$	$\dot{m}_{suc}$	$\dot{m}_{sl}$	$\dot{m}_{mc}$	fs%	MR	$(MR)_{aux}$	$(\dot{m}v)_e$	$(\dot{m}v)_{e,aux}$	$(\dot{m}v)_j$	$(\dot{m}v)_{j,aux}$	$(\phi-1)\cdot(\dot{m}v)_j$	Thrust	ϕ	ϕ_2
	psig		lbm/s										$lbm \cdot ft/s^2$					lbf		
1	10.0	7.5	.0661	.0121	.4994	.0734	.0613	.4946		10.9	7.48	5.08	104.8	4.4	69.4	10.5	1.10	1.06	1.51	1.34
2	10.0	10.0	.0666	.0143	.5194	.0915	.0771	.5299		12.9	7.95	5.38	108.8	6.7	70.2	13.8	1.20	1.12	1.55	1.37
3	10.0	12.5	.0665	.0163	.5438	.1080	.0915	.5688		14.4	8.55	5.51	114.8	9.2	70.0	17.1	1.39	1.24	1.64	1.43
4	10.0	15.0	.0664	.0183	.5435	.1171	.0989	.5760		15.4	8.68	5.42	114.9	10.8	70.1	19.1	1.39	1.40	1.64	1.41
5	10.0	17.5	.0664	.0195	.5234	.1274	.1079	.5649		17.1	8.5	5.52	112.1	12.9	70.1	20.3	1.31	1.24	1.60	1.37
6																				
7																				
8																				
9																				
10																				
11	23.2	7.5	.1053	.0120	.7912	.0528	.0408	.7267		4.9	6.90	3.39	193.3	2.3	117.8	10.5	2.34	2.33	1.64	1.53
12	23.2	10.0	.1053	.0142	.8017	.0746	.0603	.7567		7.0	7.72	4.24	200.3	4.4	117.9	13.8	2.56	2.45	1.70	1.55
13	23.2	12.5	.1065	.0165	.7999	.0911	.0746	.7680		8.5	7.20	4.53	205.6	6.5	118.9	17.2	2.70	2.64	1.73	1.56
14	23.2	15.0	.1052	.0172	.7772	.1012	.0839	.7616		9.7	7.19	4.81	209.8	8.0	117.9	17.9	2.85	2.79	1.78	1.59
15	23.2	17.5	.1071	.0197	.7830	.1106	.0969	.7663		10.4	7.16	4.60	211.9	9.6	119.7	20.5	2.95	2.86	1.77	1.60
16																				
17																				
18																				
19																				
20																				
21																				
22																				
23																				
24	35.5	12.5	.1451	.0164	.9443	.0912	.0748	.8740		7.3	6.02	4.55	282.4	6.4	162.5	17.1	3.73	3.57	1.74	1.60
25	35.5	15.0	.1451	.0176	.9581	.0988	.0812	.8922		7.8	6.15	4.60	285.6	7.5	162.5	18.3	3.84	3.79	1.76	1.62
26	35.5	17.5	.1445	.0199	.9455	.1106	.0908	.8918		8.8	6.17	4.56	282.8	9.4	161.8	20.7	3.77	3.73	1.75	1.60
27	35.5	20.0	.1442	.0211	1.0069	.1183	.0972	.9599		9.5	6.65	4.60	282.6	10.8	161.4	22.0	3.76	3.75	1.75	1.60

TABLE 1 (continued)

AR = 1.46 λ = 40 nozzle SINGLE JET

run	P_o	P_{aux}	$\dot{m}_p$	$\dot{m}_{p'}$	$\dot{m}_e$	$\dot{m}_{e,aux}$	$\dot{m}_{suc}$	$\dot{m}_{sl}$	$\dot{m}_{mc}$	fs%	MR	$(MR)_{aux}$	$(\dot{m}v)_e$	$\dot{m}_{e,aux}v_{e,aux}$	$(\dot{m}v)_j$	$\dot{m}_{j,aux}v_{j,aux}$	$(\phi-1)(\dot{m}v)_j$	Thrust	ϕ	ϕ_2
	psig		lbm/s										lbm-ft/s^2				lbf			
1	10.0	7.5	.0754	.0121	.6527	.0735	.0644	.6387		8.6	8.47	5.07	128.1	4.2	79.8	10.5	1.51	1.36	1.61	1.47
2	10.0	10.0	.0762	.0143	.6594	.0857	.0714	.6546		9.8	8.59	4.99	132.9	5.8	81.2	13.9	1.61	1.24	1.64	1.56
3	10.0	12.5	.0757	.0165	.6586	.0979	.0834	.6363		10.9	9.07	5.45	137.3	7.9	80.7	17.2	1.83	1.55	1.73	1.50
4	10.0	15.0	.0749	.0180	.6661	.1123	.0944	.6836		12.4	9.15	5.25	137.9	9.8	80.0	18.7	1.79	1.61	1.72	1.59
5	10.0	17.5	.0756	.0195	.6459	.1239	.1044	.6747		13.9	8.92	5.35	132.9	12.0	80.4	20.3	1.65	1.61	1.66	1.44
6	17.4	7.5	.0981	.0119	.8730	.0603	.0488	.8732		5.2	8.39	4.06	212.2	2.8	109.7	10.4	3.20	2.80	1.94	1.79
7	17.4	10.0	.0977	.0144	.8886	.0736	.0592	.8501		6.2	8.70	4.13	219.0	4.2	108.3	14.0	3.39	2.89	2.00	1.81
8	17.4	12.5	.0977	.0164	.8776	.0854	.0690	.8699		7.3	8.70	4.21	215.9	5.7	109.3	17.1	3.33	3.01	1.96	1.75
9	17.4	15.0	.0977	.0179	.8593	.0969	.0790	.8406		8.4	8.61	4.42	206.5	7.3	109.3	18.7	3.02	3.01	1.89	1.67
10	17.4	17.5	.0915	.0198	.8520	.1093	.0885	.8500		9.5	9.28	4.59	200.8	9.3	102.3	20.6	3.05	3.04	1.96	1.71
11	23.2	7.5	.1136	.0124	.9663	.0500	.0376	.8903	.9148	3.7	7.94	3.04	257.9	1.9	126.7	10.8	4.48	3.26	2.03	1.89
12	23.2	10.0	.1125	.0150	.9304	.0652	.0502	.9181		4.8	8.16	3.36	266.4	3.3	125.4	14.6	4.30	3.51	2.11	1.91
13	23.2	12.5	.1140	.0163	.9927	.0762	.0600	.9387		5.7	8.23	3.69	270.0	4.6	127.1	17.0	4.19	3.60	2.06	1.85
14	23.2	15.0	.1169	.0181	.9558	.0896	.0715	.9104		7.0	7.79	3.95	270.3	6.3	130.3	18.9	4.33	3.66	2.07	1.85
15	23.2	17.5	.1135	.0201	.9784	.1006	.0805	.9464		7.6	8.34	4.00	260.0	7.9	127.1	21.0	4.12	3.94	2.05	1.81
16																				
17																				
18	29.0	12.5	.1413	.0166	1.0941	.0782	.0616	.9734	1.0928	5.5	6.90	3.70	307.3	4.7	157.9	17.3	4.66	4.22	1.95	1.78
19	29.0	15.0	.1408	.0184	1.0335	.0902	.0718	.9845		6.4	7.00	3.91	307.4	6.3	158.0	19.2	4.66	4.25	1.95	1.77
20	29.0	17.5	.1410	.0199	1.0899	.0970	.0772	.9750		6.9	6.91	3.89	296.9	7.3	158.2	20.7	4.32	4.10	1.88	1.70
21	29.0	20.0	.1408	.0214	1.0899	.0995	.0782	1.0073	1.1221	6.8	7.16	3.46	298.9	7.7	158.0	22.3	4.37	4.19	1.89	1.70
22																				
23																				
24	35.5	12.5	.1607	.0165	1.0885	.0723	.0559	.9886	1.1273	4.9	6.15	3.40	338.4	4.0	179.1	17.2	4.95	4.50	1.99	1.75
25	35.5	15.0	.1618	.0179	1.0925	.0891	.0667	.9904		5.8	6.15	3.72	337.7	5.5	180.9	18.7	4.88	4.41	1.87	1.72
26	35.5	17.5	.1617	.0198	1.0918	.0929	.0731	1.0052	1.1633	6.3	6.20	3.68	335.1	6.7	180.9	20.7	4.78	4.41	1.85	1.69
27	35.5	20.0	.1618	.0214	1.1121	.1019	.0805	1.0318		6.8	6.37	3.71	350.5	8.1	181.0	22.3	5.23	4.78	1.94	1.76

TABLE 1 (continued)

AR = 1.46 λ = 40 nozzle EIGHT-JET

run	P_o	P_{aux}	$\dot{m}_p$	$\dot{m}_{p'}$	$\dot{m}_e$	$\dot{m}_{e,aux}$	$\dot{m}_{suc}$	$\dot{m}_{tt}$	$\dot{m}_{mc}$	fs%	MR	$(MR)_{aux}$	$(inv)_c$	$(inv)_{s,aux}$	$(inv)_j$	$(inv)_{j,aux}$	$(\frac{\phi}{\phi}-1)\cdot(inv)_j$	Thrust	ϕ	ϕ_2
	psig		lbm/s										lbm-ft/s²					lbf		
1	10.0	7.5	.0682	.0126	.6009	.0698	.0572	.5889		8.7	8.64	4.52	108.0	3.9	71.1	10.8	1.14	.84	1.51	1.35
2	10.0	10.0	.0682	.0145	.5723	.0920	.0715	.5816		11.9	8.52	5.33	104.6	6.7	71.9	14.0	1.00	.84	1.45	1.29
3	10.0	12.5	.0682	.0161	.5880	.1054	.0892	.6090		13.2	8.98	5.52	106.2	8.7	71.7	16.8	1.09	.93	1.48	1.30
4	10.0	15.0	.0680	.0179	.6148	.1164	.0982	.6450		13.8	9.49	5.47	111.0	10.6	71.5	18.7	1.23	1.06	1.55	1.35
5	10.0	17.5	.0681	.0198	.5789	.1260	.1062	.6170		15.5	9.06	5.36	102.8	12.5	71.6	20.6	.97	1.06	1.44	1.25
6																				
7																				
8																				
9																				
10																				
11	23.2	7.5	.1076	.0124	.8464	.0666	.0542	.7930		6.0	7.37	4.37	211.4	3.4	120.2	10.8	2.85	1.99	1.76	1.64
12	23.2	10.0	.1072	.0147	.8429	.0803	.0657	.8049		7.2	7.48	4.98	210.3	5.0	120.1	14.2	2.80	2.17	1.75	1.60
13	23.2	12.5	.1065	.0164	.8343	.0912	.0748	.8026		8.2	7.53	4.55	207.5	6.5	119.3	17.1	2.74	2.33	1.74	1.57
14	23.2	15.0	.1065	.0180	.8393	.1020	.0840	.8469		9.1	7.67	4.67	208.9	8.1	119.3	18.7	2.78	2.23	1.75	1.57
15	23.2	17.5	.1065	.0198	.8376	.1121	.0922	.8233		9.9	7.76	4.65	209.0	9.9	119.1	20.6	2.79	2.24	1.75	1.57
16																				
17																				
18																				
19																				
20																				
21																				
22																				
23																				
24	35.5	12.5	.1485	.0164	.9722	.0746	.0583	.8920		5.7	5.94	3.55	288.3	4.4	166.2	17.1	3.74	2.24	1.73	1.60
25	35.5	15.0	.1488	.0180	.9754	.0863	.0683	.8949		6.6	6.01	3.80	291.8	5.9	166.6	18.8	3.89	2.29	1.75	1.61
26	35.5	17.5	.1486	.0198	.9800	.0981	.0782	.9096		7.4	6.12	3.94	293.0	7.5	166.5	20.6	3.93	3.11	1.76	1.61
27	35.5	20.0	.1474	.0214	.9810	.1100	.0867	.9223		8.3	6.27	4.15	297.4	9.5	166.2	22.3	4.10	3.07	1.80	1.64

TABLE 1 (continued)

AR = 1.26 λ = 20 nozzle SINGLE JET

run	P_o	P_{aux}	$\dot{m}_p$	$\dot{m}_{p'}$	$\dot{m}_o$	$\dot{m}_{o,aux}$	$\dot{m}_{suc}$	$\dot{m}_{el}$	$\dot{m}_{mc}$	fs%	MR	$(MR)_{max}$	$(inv)_o$	$(ind)_{o,max}$	$(inv)_j$	$(ind)_{j,max}$	$(\phi-1)\frac{(inv)_j}{(ind)_j}$	Thrust	ϕ	ϕ_2
	psig		lbm/s										lbm-ft/s^2					lbf		
1	10.0	7.5	.0734	.0078	.4679	.0348	.0289	.3614		6.2	4.93	3.44	114.3	.9	77.2	6.8	1.15	1.00	1.48	1.37
2	10.0	10.0	.0728	.0092	.4055	.0429	.0388	.3665		7.7	5.63	3.69	115.8	1.4	76.6	8.7	1.20	1.10	1.51	1.37
3	10.0	12.5	.0730	.0100	.4108	.0495	.0495	.3873		10.7	5.31	4.93	117.6	2.7	76.8	10.4	1.27	1.32	1.53	1.38
4	10.0	15.0	.0728	.0107	.4240	.0682	.0586	.4055	.4607	11.4	5.56	5.48	123.7	3.3	77.0	11.1	1.46	1.25	1.61	1.44
5	10.0	17.5	.0728	.0116	.4199	.0681	.0585	.4036		11.9	5.54	4.87	121.5	3.6	76.8	12.1	1.39	1.50	1.58	1.41
6	17.4	7.5	.0968	.0075	.5785	.0252	.0177	.4344		3.3	4.49	2.37	168.4	.5	108.4	6.5	1.89	1.89	1.55	1.47
7	17.4	10.0	.0968	.0088	.5209	.0349	.0260	.4501		4.8	4.65	2.96	172.9	1.0	108.3	8.5	2.00	1.91	1.60	1.49
8	17.4	12.5	.0968	.0100	.5135	.0434	.0335	.4492		5.9	4.64	3.25	168.4	1.4	108.1	10.4	1.87	1.90	1.56	1.43
9	17.4	15.0	.0966	.0107	.5236	.0490	.0383	.4651	.5100	6.8	4.81	3.56	174.2	1.9	108.2	11.2	2.05	1.93	1.61	1.48
10	17.4	17.5	.0966	.0116	.5213	.0574	.0468	.4745		8.1	4.87	3.97	173.5	2.6	108.0	12.1	2.04	2.02	1.61	1.47
11	23.2	7.5	.1153	.0073	.5433	.0274	.0200	.4415		3.6	3.87	2.74	194.8	.6	129.7	6.3	1.71	1.44	1.43	1.36
12	23.2	10.0	.1157	.0089	.5431	.0339	.0249	.4523		4.4	3.91	2.78	196.6	.9	129.6	8.6	1.78	1.53	1.44	1.36
13	23.2	12.5	.1155	.0100	.5448	.0393	.0293	.4586		5.1	3.97	2.94	188.9	1.2	129.2	10.4	1.85	1.56	1.46	1.36
14	23.2	15.0	.1160	.0100	.5308	.0413	.0313	.4961	.6335	5.1	4.28	3.13	206.9	1.3	129.8	11.2	2.37	2.28	1.59	1.49
15	23.2	17.5	.1155	.0116	.5468	.0530	.0414	.4861		6.9	4.21	3.58	196.9	2.2	129.2	12.1	2.10	2.42	1.52	1.41
16	29.0	7.5	.1396	.0074	.6514	.0464	.0391	.5339		5.6	3.98	5.32	248.6	1.6	156.4	6.4	2.87	2.60	1.59	1.57
17	29.0	10.0	.1392	.0083	.6587	.0538	.0455	.5630		6.5	4.09	5.47	249.2	2.3	155.7	8.0	2.90	2.79	1.60	1.57
18	29.0	12.5	.1390	.0092	.6544	.0589	.0492	.5646		7.0	4.06	5.34	248.1	2.7	155.5	9.6	2.87	2.90	1.60	1.52
19	29.0	15.0	.1390	.0099	.6727	.0625	.0526	.5863	.7164	7.3	4.22	5.29	262.6	3.1	155.3	10.3	3.33	2.87	1.69	1.60
20	29.0	17.5	.1388	.0107	.6726	.0710	.0602	.5940		8.2	4.28	5.61	263.5	3.9	155.3	11.2	3.36	2.84	1.70	1.61
21	35.5	7.5	.1590	.0073	.6321	.0322	.0209	.4980		3.8	3.13	3.40	253.2	.8	177.8	6.4	2.35	2.10	1.43	1.38
22	35.5	10.0	.1584	.0083	.6305	.0296	.0213	.4934		3.3	3.12	2.57	254.9	.7	177.3	8.0	2.41	2.20	1.49	1.38
23	35.5	12.5	.1578	.0093	.6313	.0290	.0222	.4957		3.0	3.12	2.12	254.0	.7	176.5	9.7	2.40	2.40	1.44	1.37
24	35.5	15.0	.1567	.0099	.6649	.0372	.0295	.5377	.7237	3.9	3.42	2.75	276.4	1.1	175.4	10.3	3.14	2.68	1.58	1.50
25	35.5	17.5	.1569	.0109	.6279	.0445	.0321	.5200		5.1	3.21	3.07	261.9	1.5	175.4	11.4	2.89	2.90	1.49	1.41
26	35.5	20.0	.1576	.0118	.6598	.0439	.0311	.5244		4.6	3.33	2.64	262.3	1.4	176.2	12.3	2.90	2.90	1.53	1.44
27																				

TABLE 1 (continued)

AR = 1.26 λ = 20 nozzle EIGHT-JET

run	P_o	P_{aux}	$\dot{m}_p$	$\dot{m}_{p'}$	$\dot{m}_s$	$\dot{m}_{s,aux}$	$\dot{m}_{suc}$	$\dot{m}_{sl}$	$\dot{m}_{mc}$	fs%	MR	$(MR)_{min}$	$(inv)_s$	$(inv)_{s,min}$	$(inv)_j$	$(inv)_{j,min}$	$(\phi-1)\cdot(inv)_j$	Thrust	ϕ	ϕ_2
	psig		lbm/s										lbm-ft/s^2				lbf			
1	10.0	7.5	.0677	.0077	.3467	.0518	.0441	.3221		11.3	4.76	5.69	829	2.1	71.3	6.7	.36	.27	1.16	1.09
2	10.0	10.0	.0681	.0089	.3435	.0581	.0451	.3245		11.6	4.71	5.06	82.6	2.3	71.8	8.6	.34	.36	1.15	1.06
3	10.0	12.5	.0680	.0098	.3386	.0645	.0547	.3283		13.9	4.79	5.38	81.5	3.2	71.8	10.2	.31	.36	1.14	1.04
4	10.0	15.0	.0680	.0107	.3566	.0727	.0620	.3506		14.8	5.16	5.81	88.1	4.2	71.3	11.2	.51	.36	1.23	1.11
5	10.0	17.5	.0677	.0116	.3433	.0778	.0663	.349		16.2	5.05	5.74	85.6	4.3	71.6	12.1	.44	.36	1.20	1.08
6																				
7																				
8																				
9																				
10																				
11	23.2	7.5	.1086	.0025	.4995	.0368	.0293	.4202		5.6	3.87	3.92	168.0	1.0	121.8	6.5	1.44	1.23	1.38	1.32
12	23.2	10.0	.1084	.0091	.4909	.0428	.0336	.4461		6.4	3.94	3.68	162.1	1.4	121.6	8.8	1.26	1.08	1.28	1.25
13	23.2	12.5	.1082	.0100	.4852	.0483	.0382	.4192		7.3	3.88	3.82	163.5	1.8	121.3	10.4	1.31	1.17	1.35	1.26
14	23.2	15.0	.1082	.0107	.4765	.0552	.0445	.4418		8.5	3.94	4.16	158.6	2.4	121.3	11.1	1.16	1.17	1.31	1.22
15	23.2	17.5	.1082	.0116	.4674	.0592	.0476	.4068		9.2	3.76	4.11	149.7	2.7	121.1	12.1	.89	1.23	1.24	1.15
16																				
17																				
18																				
19																				
20																				
21																				
22																				
23	35.5	12.5	.1483	.0092	.6017	.0459	.0387	.4871		5.3	3.89	3.65	246.0	1.4	166.2	9.6	2.48	1.93	1.48	1.41
24	35.5	15.0	.1485	.0100	.6101	.0492	.0373	.5009		6.1	3.37	3.94	251.4	1.9	165.9	10.4	2.65	1.92	1.52	1.44
25	35.5	17.5	.1483	.0110	.6123	.0522	.0412	.5082		6.3	3.41	3.75	254.1	2.1	165.7	11.4	2.75	1.98	1.53	1.45
26	35.5	20.0	.1480	.0118	.6120	.0561	.0443	.5083		6.8	3.44	3.75	254.9	2.4	165.5	12.3	2.78	2.04	1.54	1.45
27																				

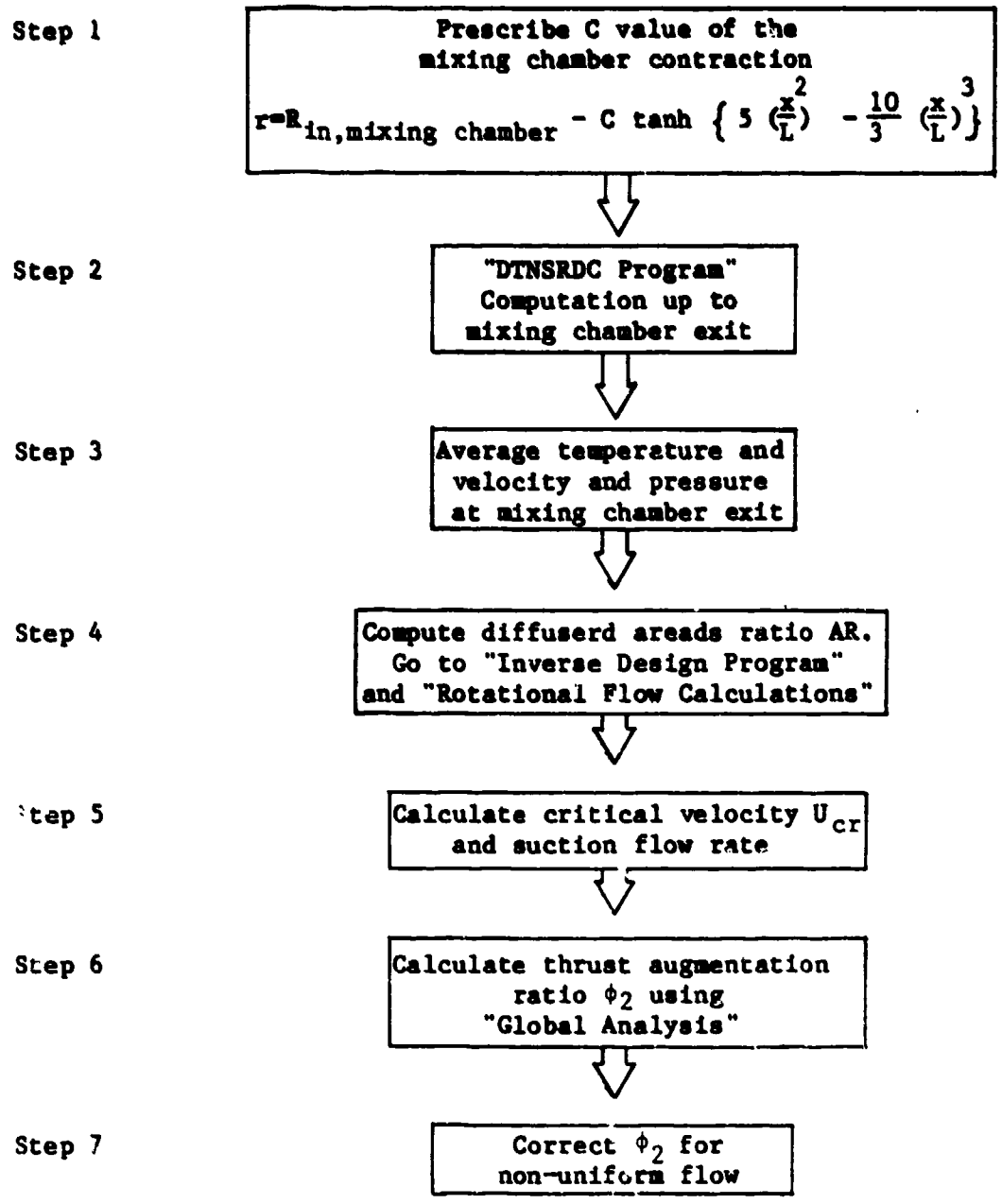

Figure 1. Block-diagram showing the major steps in ejector analysis.

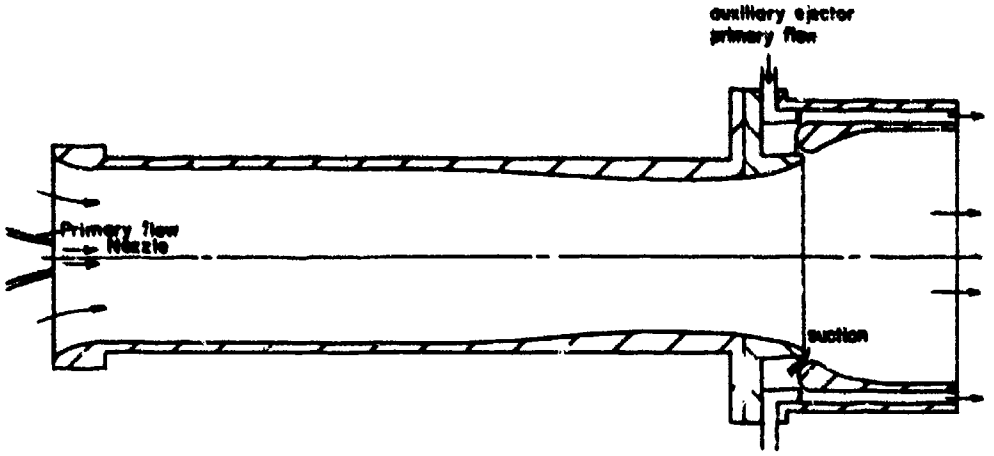

Figure 2. Geometry of ejector with diffuser area ratio of 2.2, $\lambda = 40$, $(L/D)_{overall} = 5.26$ and 16 jets for auxiliary ejector.

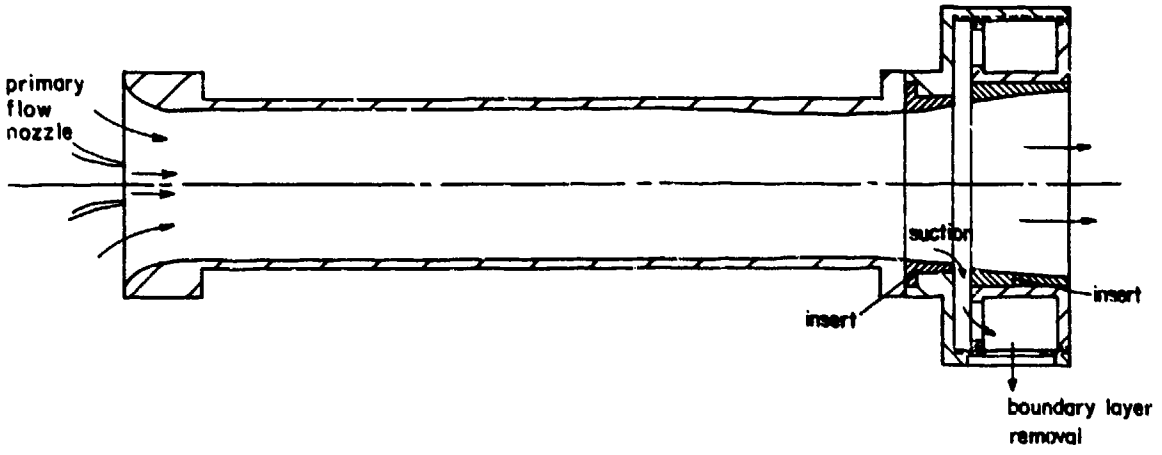

Figure 3. Geometry of ejector with diffuser area ratio of 1.33, $\lambda = 40$, $(L/D)_{overall} = 6.09$.

(Inserts were replaced to form diffuser area ratio of 1.46, $\lambda = 40$ and $(L/D)_{overall} = 6.16$.

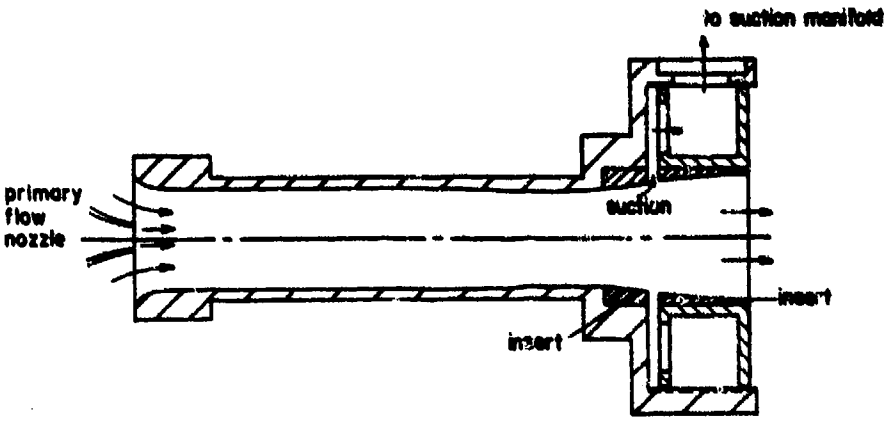

Figure 4. Geometry of the ejector with diffuser area ratio of 1.26, $\lambda = 20$, $(L/D)_{overall} = 6.02$

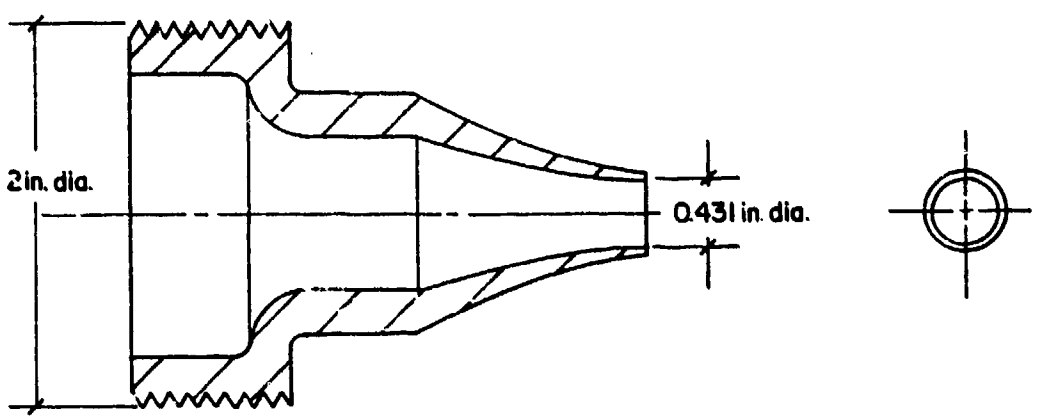

Figure 5. Single-jet converging nozzle.

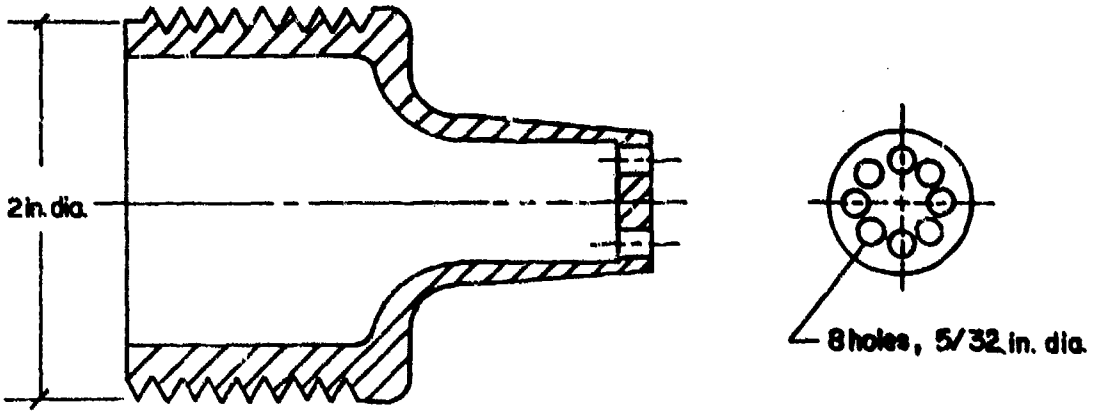

Figure 6. Eight-jet converging nozzle.

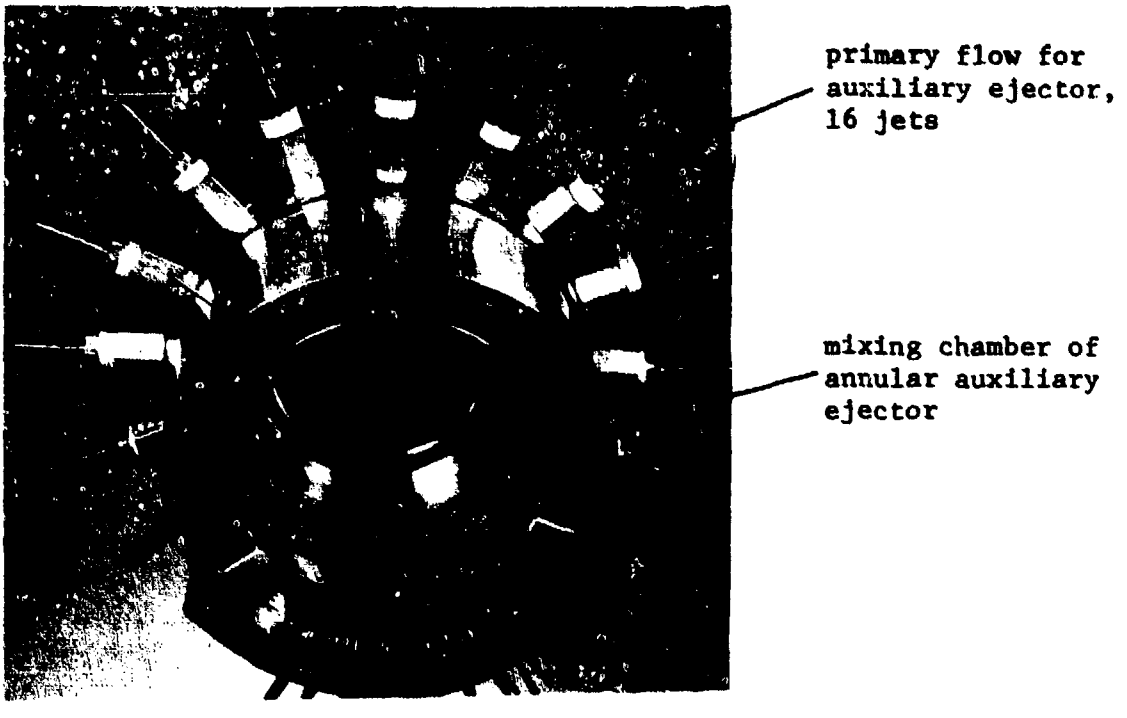

Figure 7. Sixteen-jet annular auxiliary ejector.

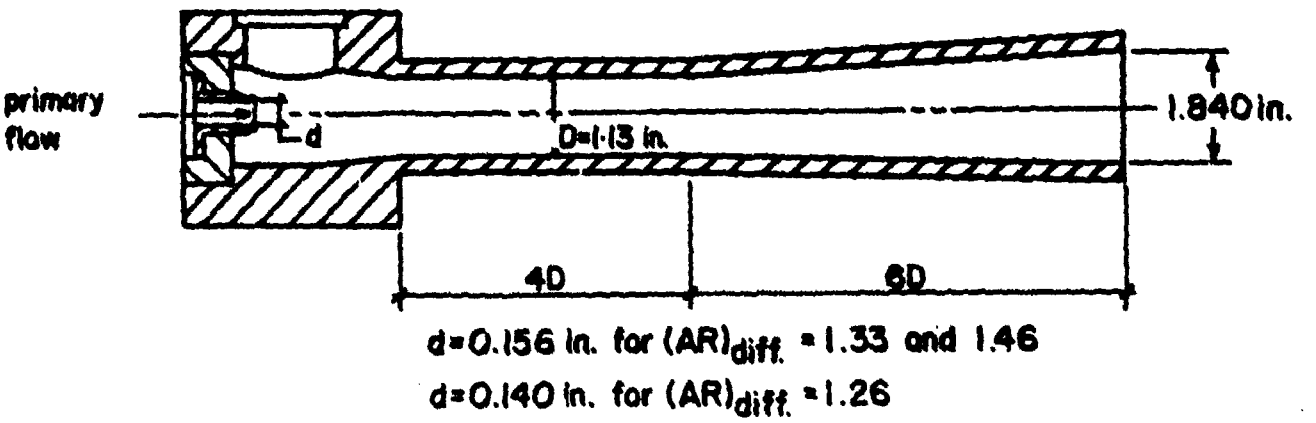

Figure 8. Single-jet auxiliary ejector.

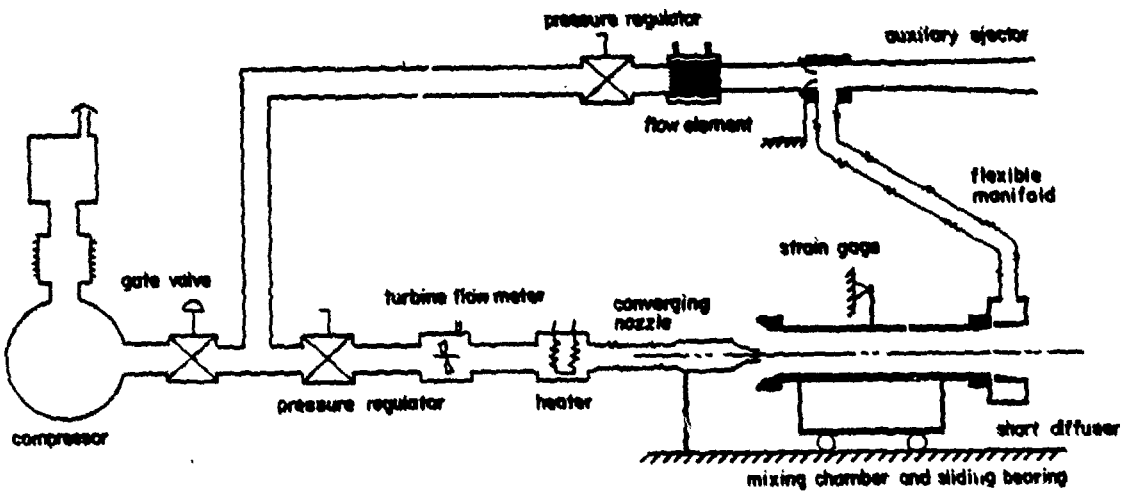

Figure 9. Schematic of test setup.

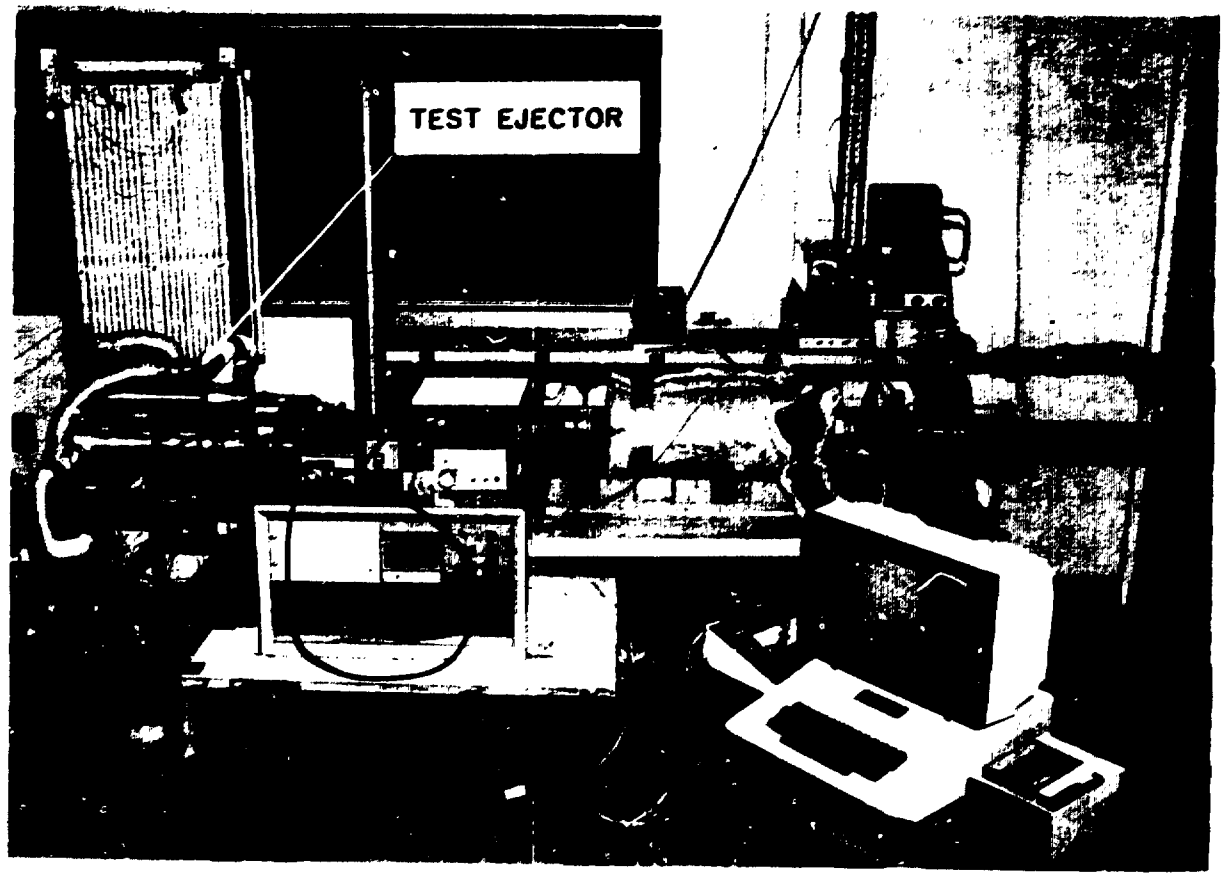

Figure 10. Overall view of the ejector performance test setup.

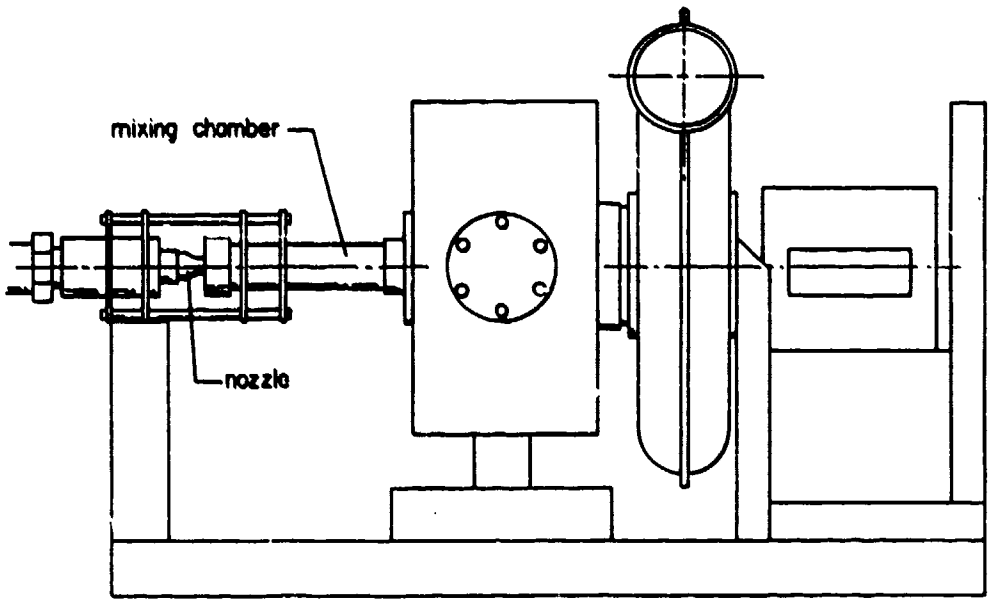

Figure 11. Front view of the mixing chamber test rig for diffuser inlet velocity profile.

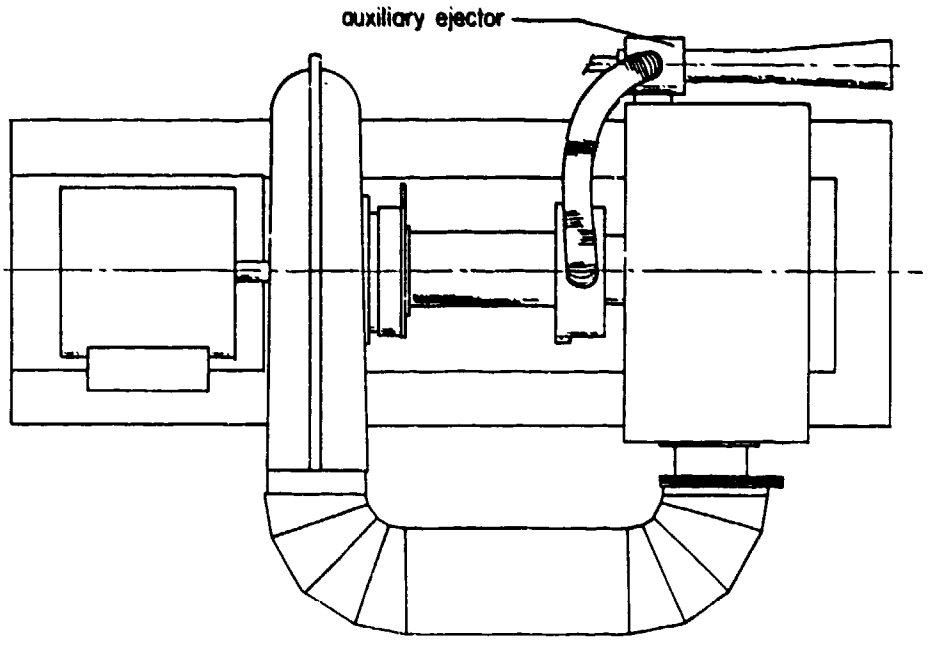

Figure 12. Top view of the auxiliary ejector test rig for optimizing nozzle diameter.

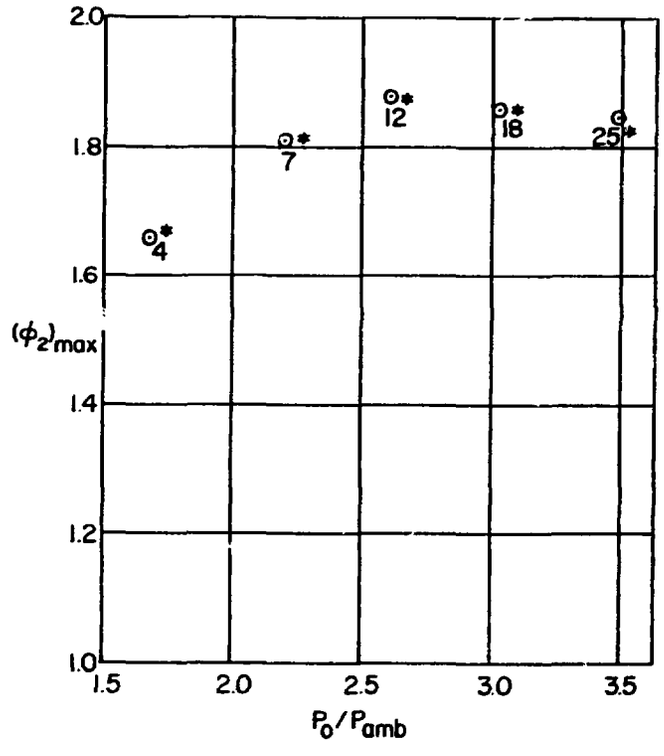

Figure 13. Loci of $(\phi_2)_{max}$ vs. primary nozzle pressure ratio. AR = 1.33, λ = 40, single-jet nozzle.

*Number adjacent to data point refers to run number listed in Table 1.

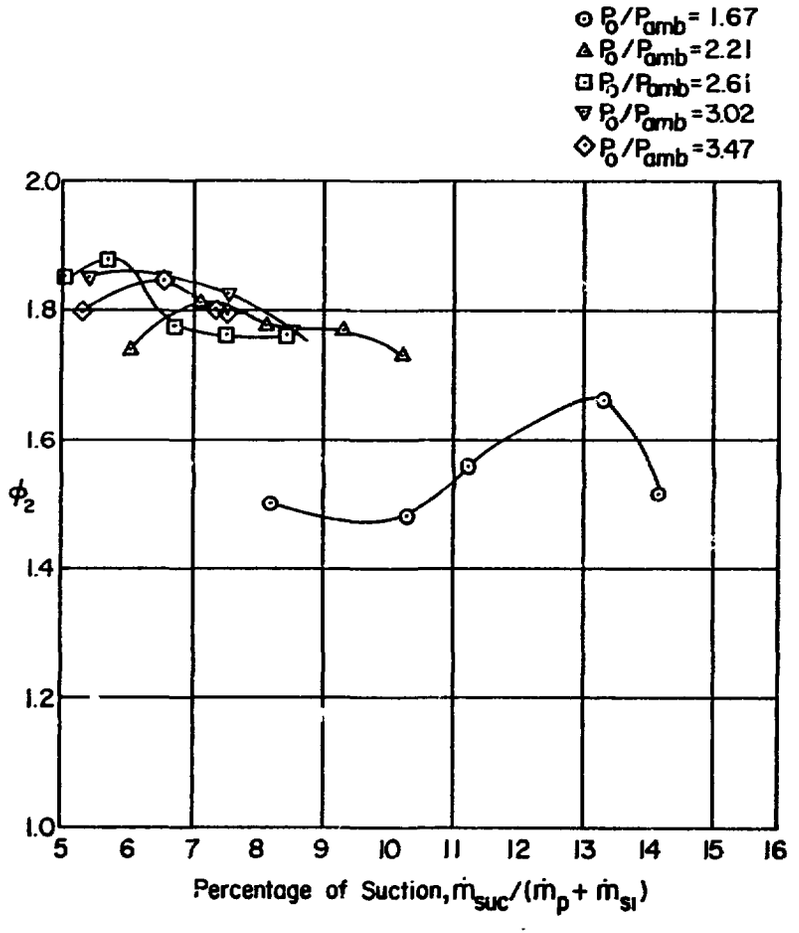

Figure 14. Parametric performance curve ϕ_2 vs boundary layer suction percentage. AR = 1.33, λ = 40, single-jet nozzle.

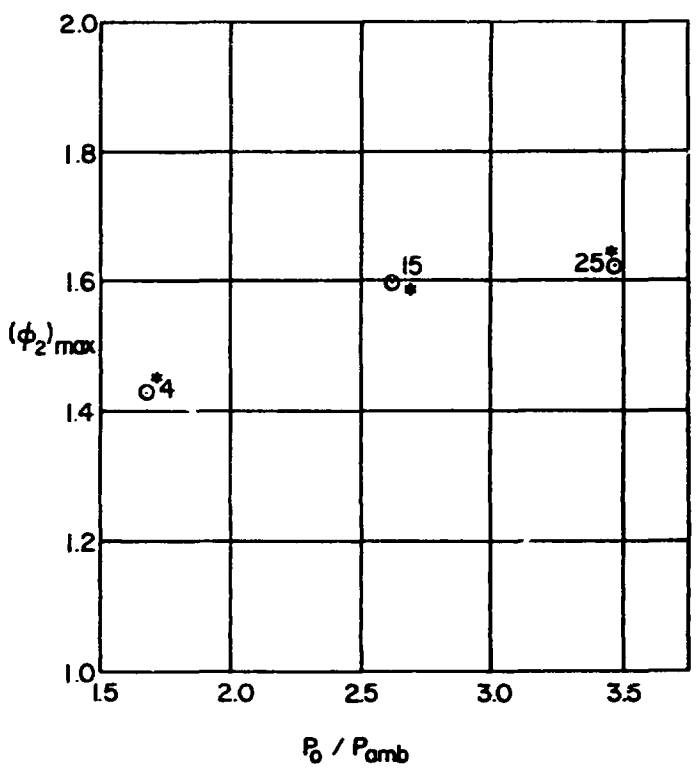

Figure 15. Loci of $(\phi_2)_{max}$ vs primary nozzle pressure ratio. AR = 1.33, λ = 40, eight-jet nozzle.

*Number adjacent to data point refers to run number listed in Table 1.

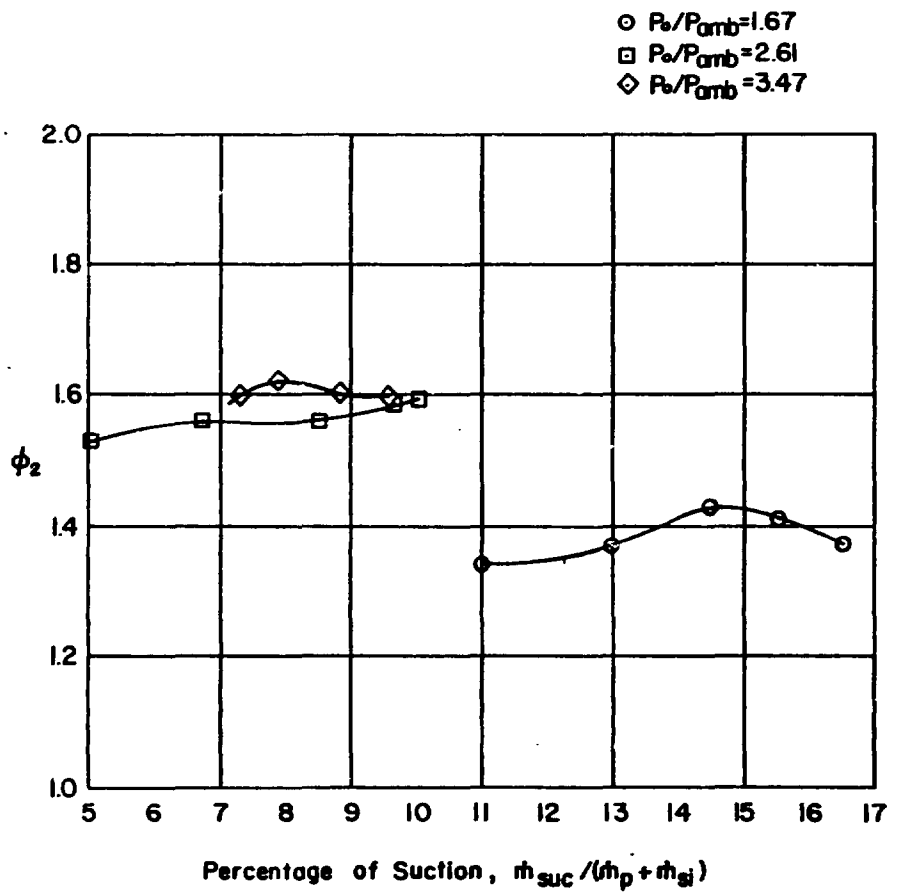

Figure 16. Parametric performance curve ϕ_2 vs boundary layer suction percentage. AR = 1.33, λ = 40, eight-jet nozzle.

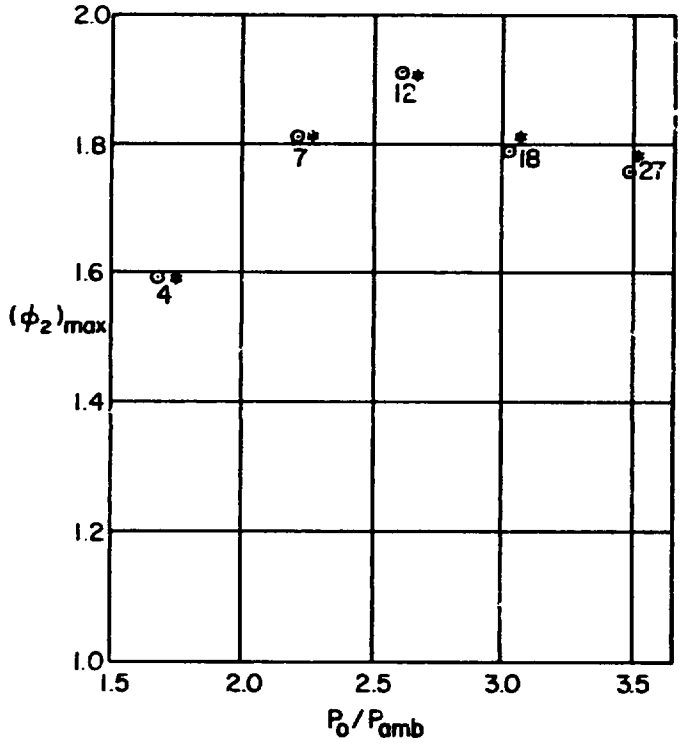

Figure 17. Loci of $(\phi_2)_{max}$ vs primary ratio. AR = 1.46, λ = 40 single-jet nozzle.

*Number adjacent to data point refers to run number listed in Table 1.

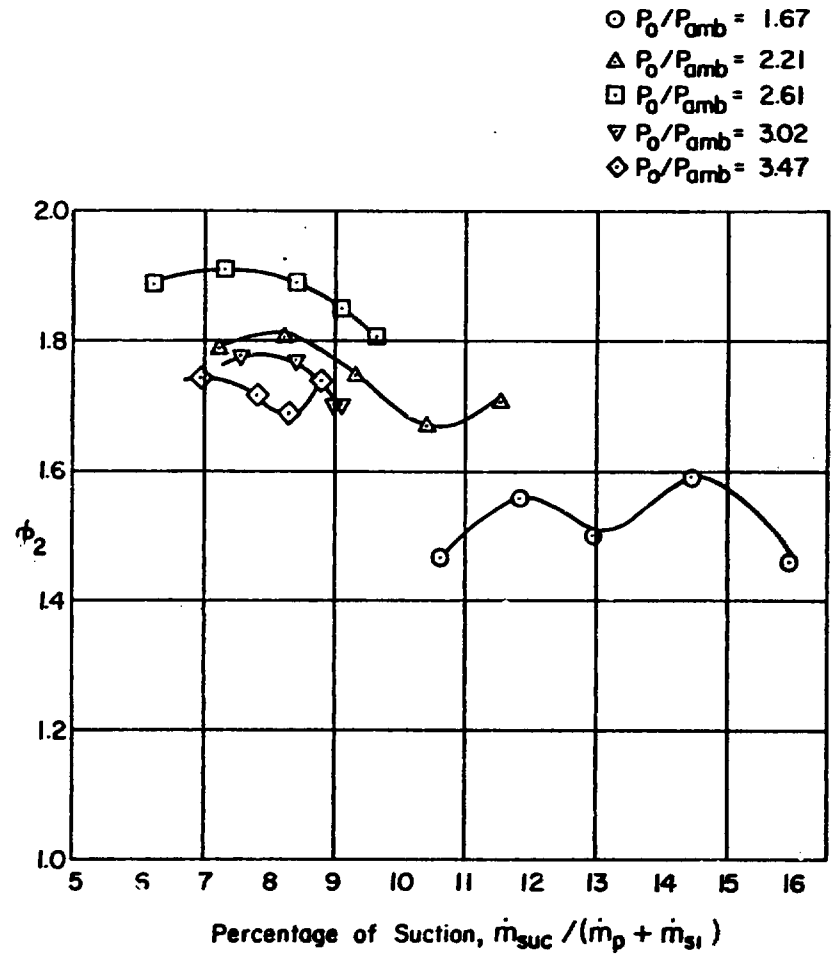

Figure 18. Parametric performance curve ϕ_2 vs boundary layer suction percentage. AR = 1.46, λ = 40, single-jet nozzle.

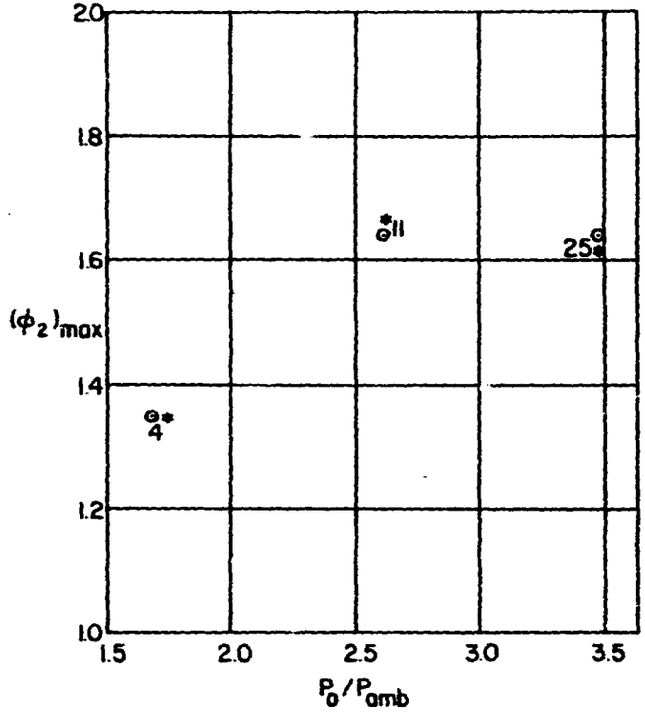

Figure 19. Loci of $(\phi_2)_{max}$ vs primary nozzle pressure ratio. AR = 1.46, λ = 40, eight-jet nozzle.

*Number adjacent to data point refers to run number listed in Table 1.

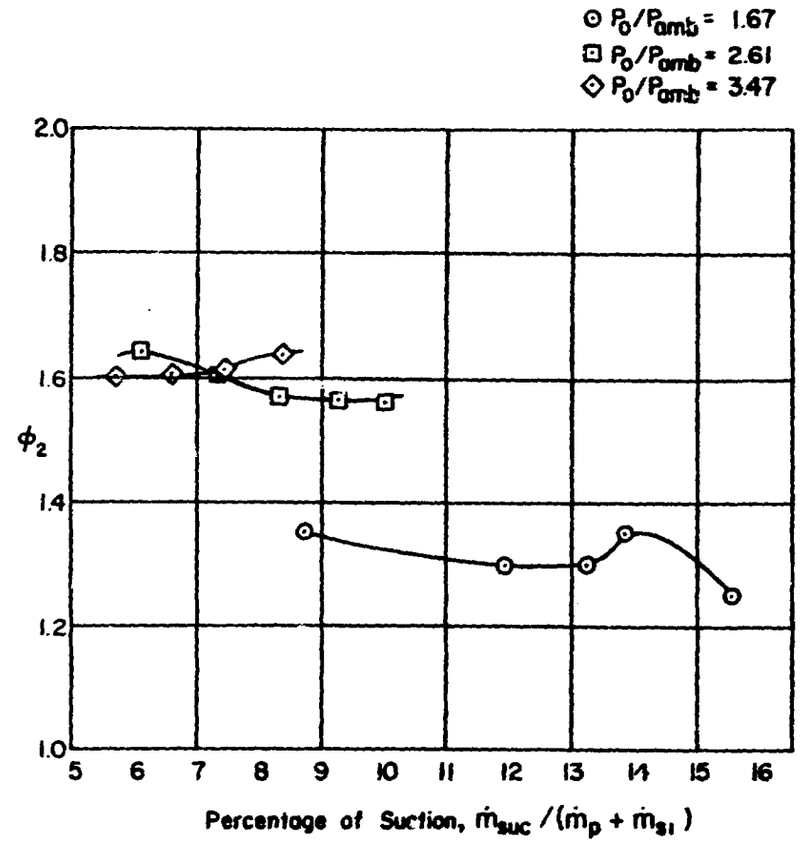

Figure 20. Parametric performance curve ϕ_2 vs boundary layer suction percentage. AR = 1.46, λ = 40, eight-jet nozzle.

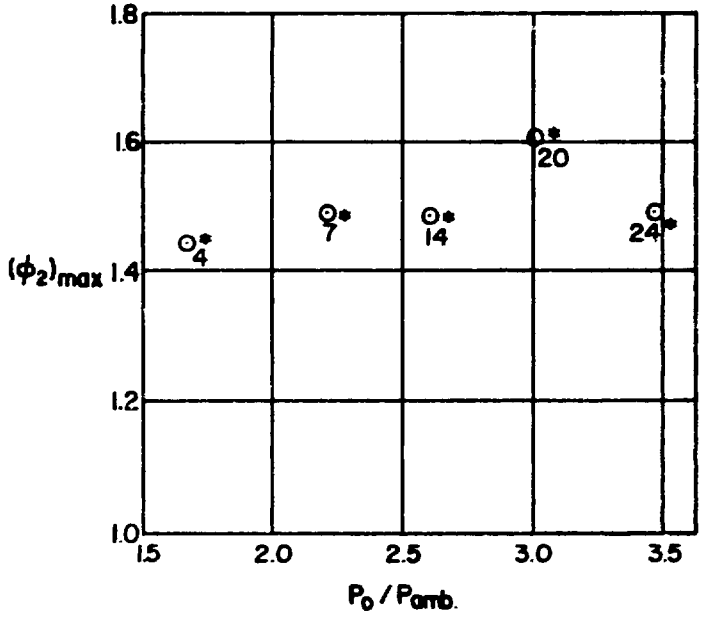

Figure 21. Loci of $(\phi_2)_{max}$ vs primary nozzle pressure ratio. AR = 1.26, λ = 20, single-jet nozzle.

*Number adjacent to data point refers to run number listed in Table 1.

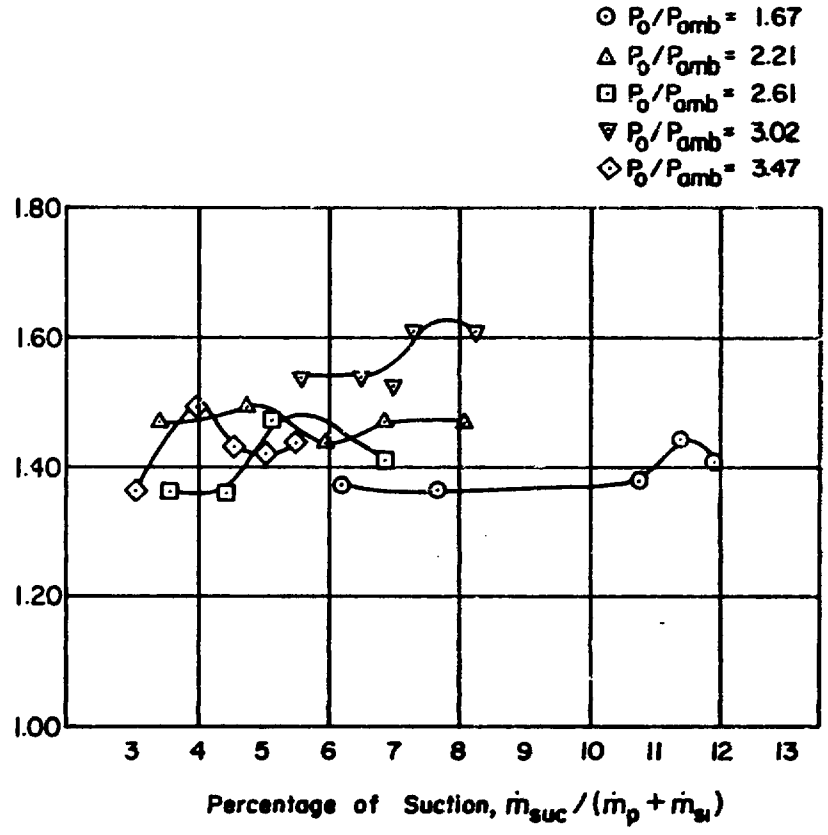

Figure 22. Parametric performance curve ϕ_2 vs boundary layer suction percentage. AR = 1.26, λ = 20, single-jet nozzle.

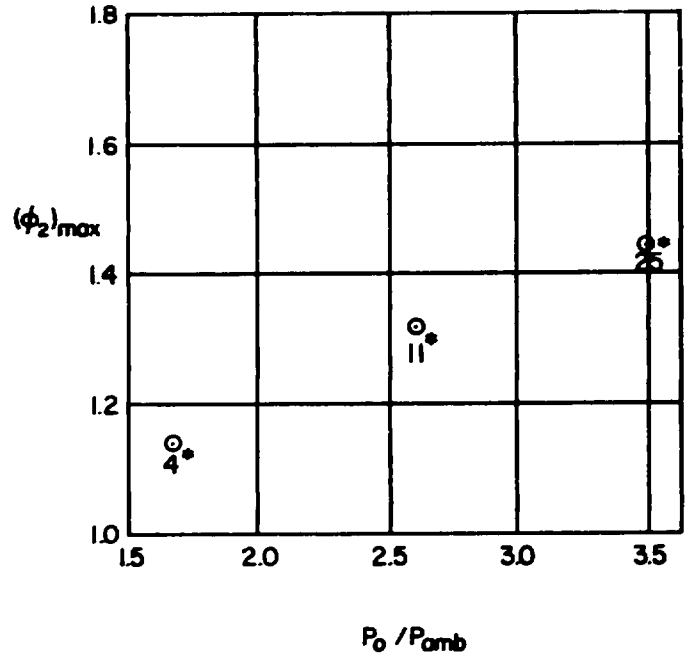

Figure 23. Loci of $(\phi_2)_{max}$ vs primary nozzle pressure ratio. AR = 1.26, λ = 20, eight-jet nozzle.

*Number adjacent to data point refers to run number listed in Table 1.

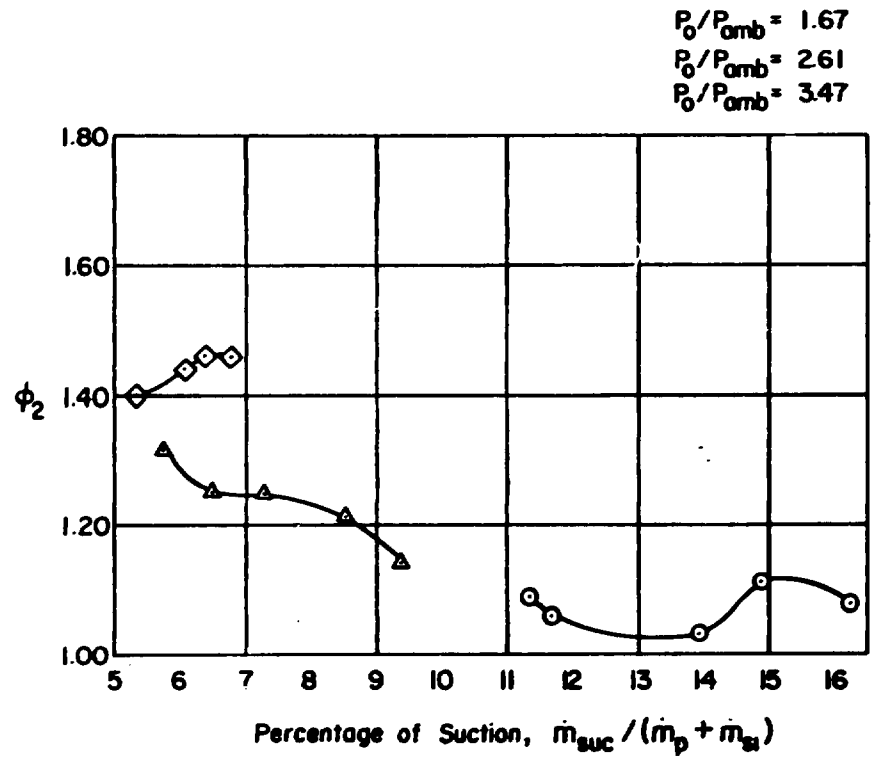

Figure 24. Parametric performance curve ϕ_2 vs boundary layer suction percentage. AR = 1.26, λ = 20, eight-jet nozzle.

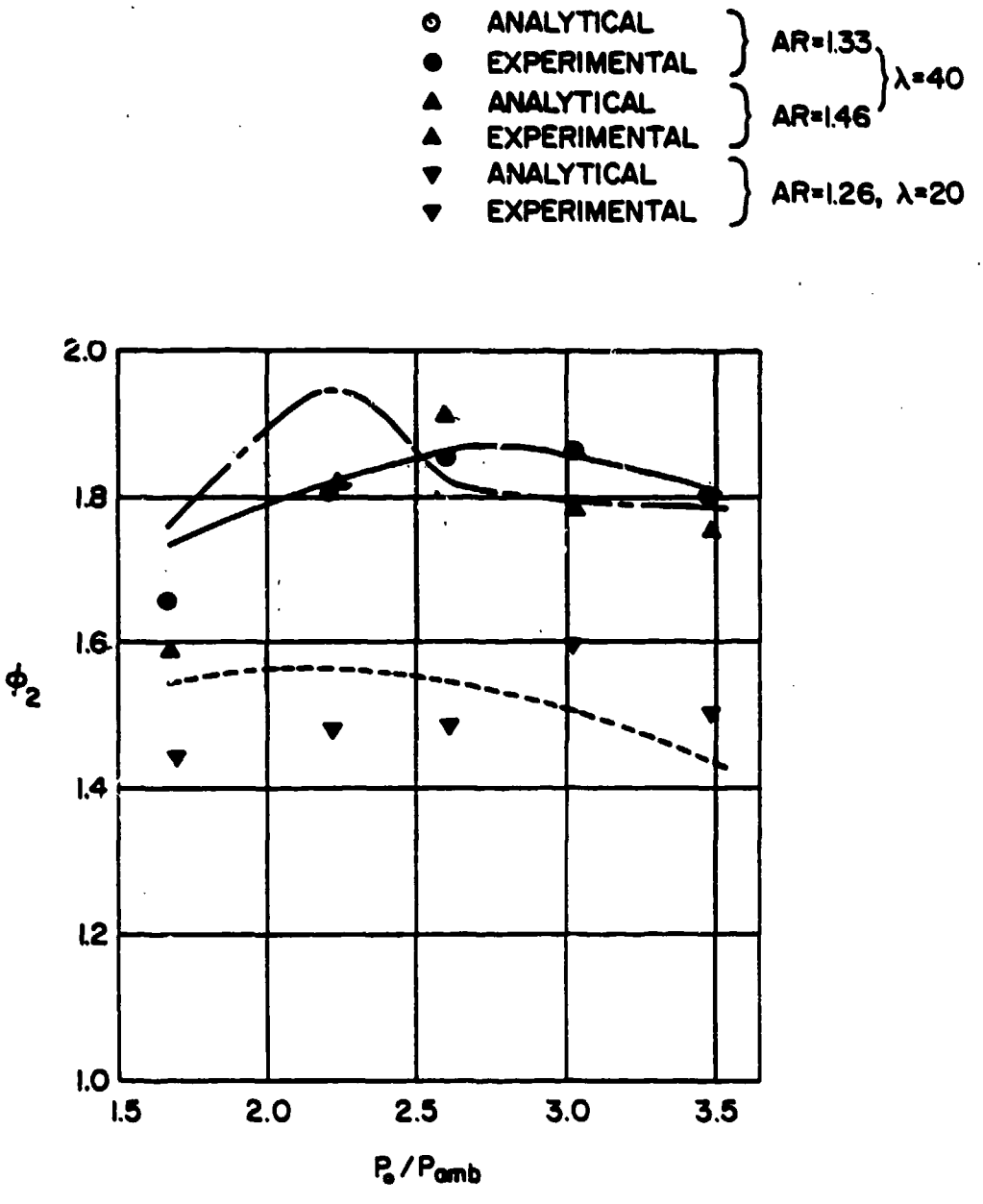

Figure 25. Comparison of analytically and experimentally determined ϕ_2 values at various P_o/P_{amb} ratios.

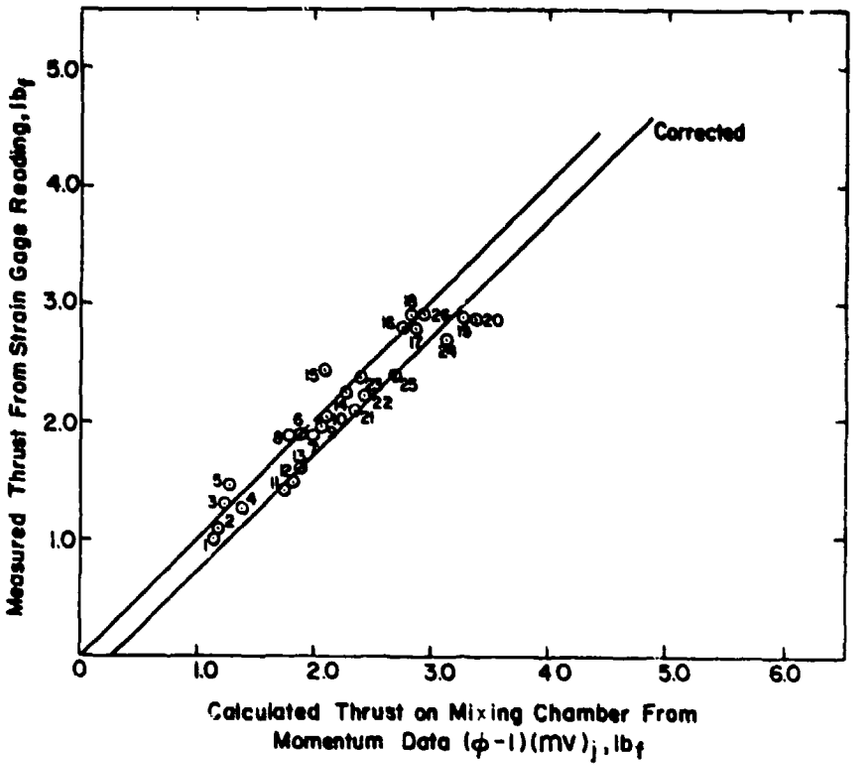

Figure 26. Comparison of measured and computed thrust on mixing chamber, AR = 1.26, λ = 20, single-jet nozzle.

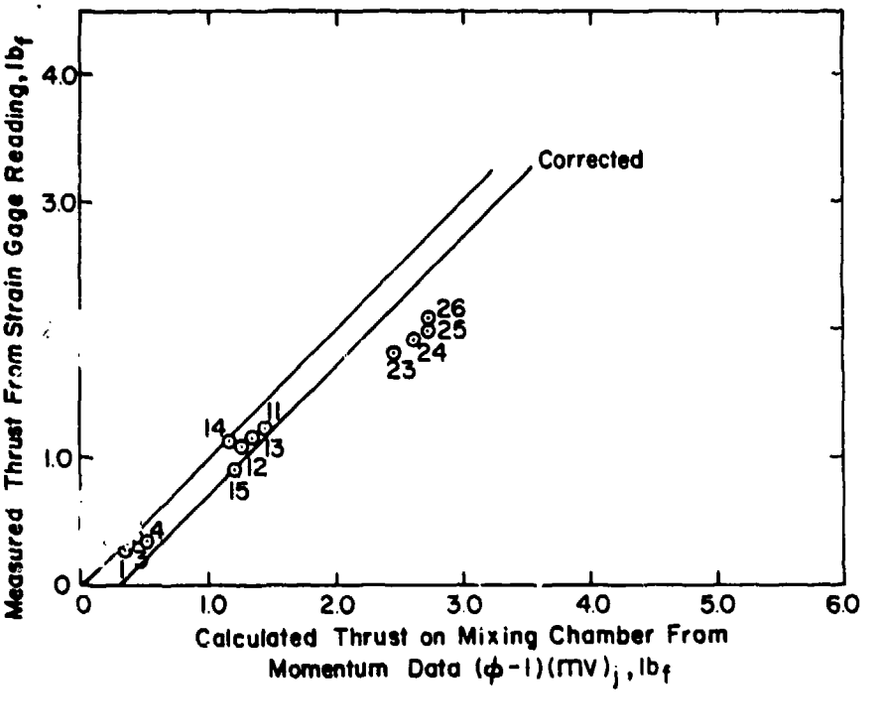

Figure 27. Comparison of measured and computed thrust on mixing chamber, AR = 1.26, λ = 20, eight-jet nozzle.

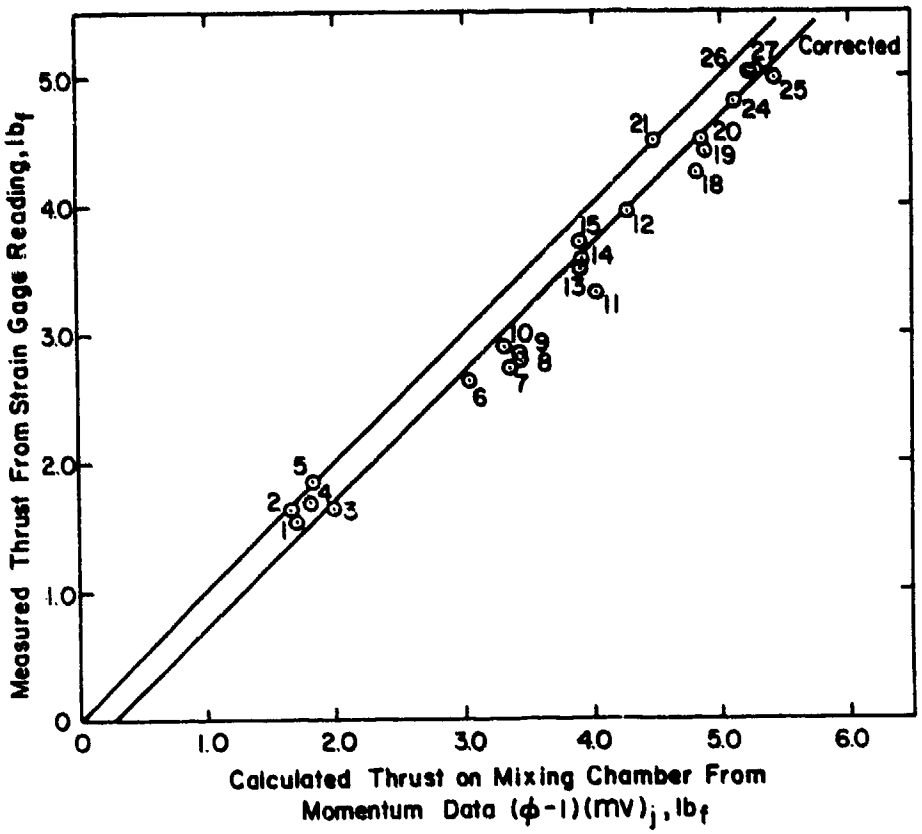

Figure 28. Comparison of measured and computed thrust on mixing chamber, AR = 1.33, λ = 40, single-jet nozzle.

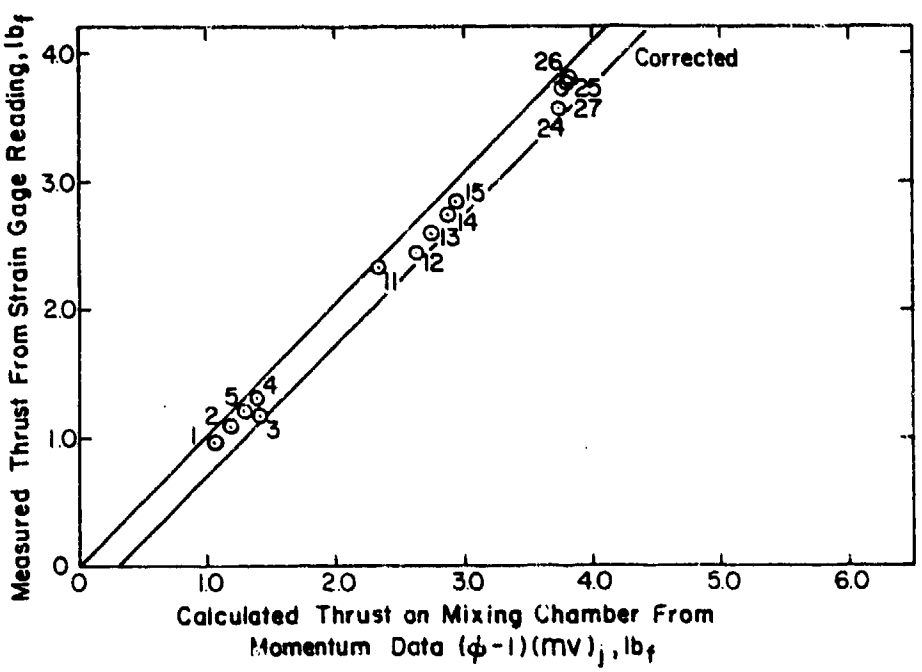

Figure 29. Comparison of measured and computed force on mixing chamber, AR = 1.33, λ = 40, eight-jet nozzle.

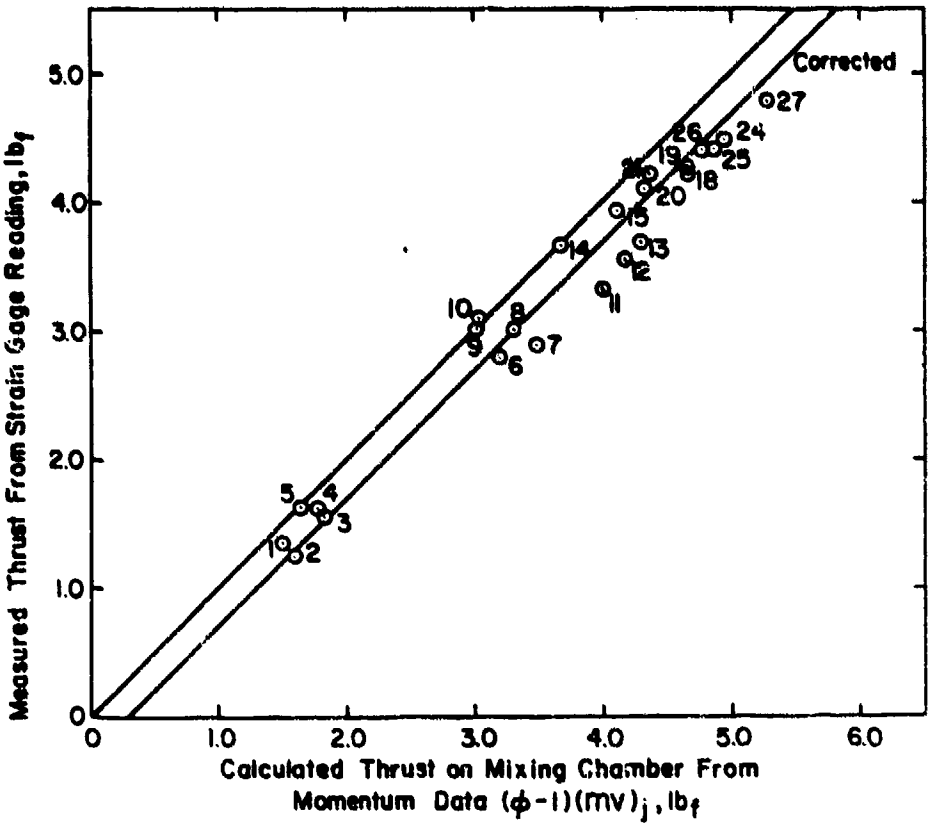

Figure 30. Comparison of measured and computed thrust on mixing chamber, AR = 1.46, λ = 40, single-jet nozzle.

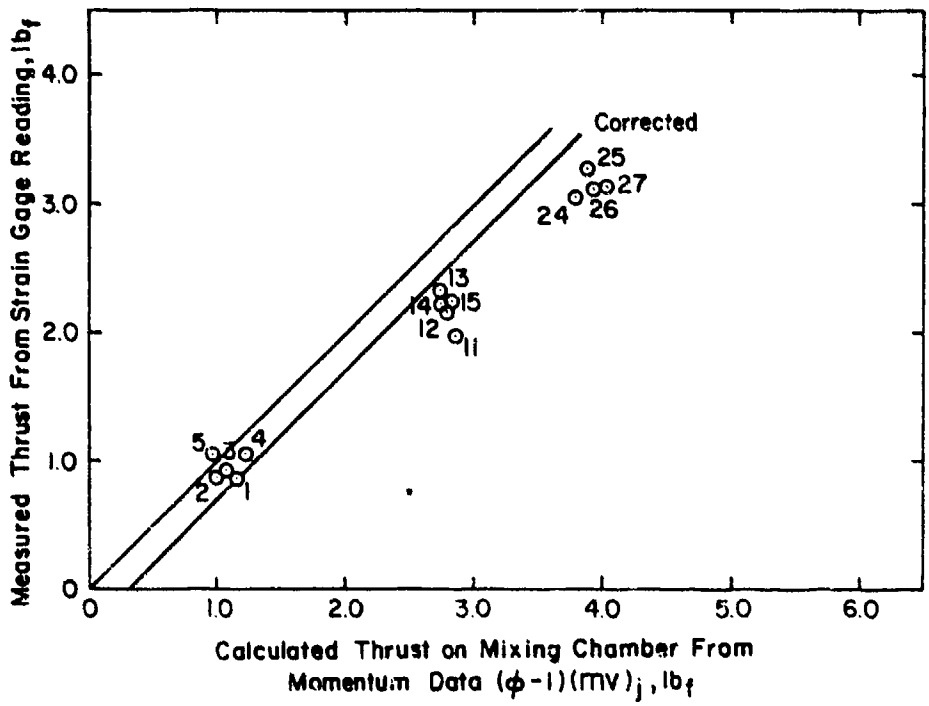

Figure 31. Comparison of measured and computed thrust on mixing chamber, AR = 1.46, λ = 40, eight-jet nozzle.

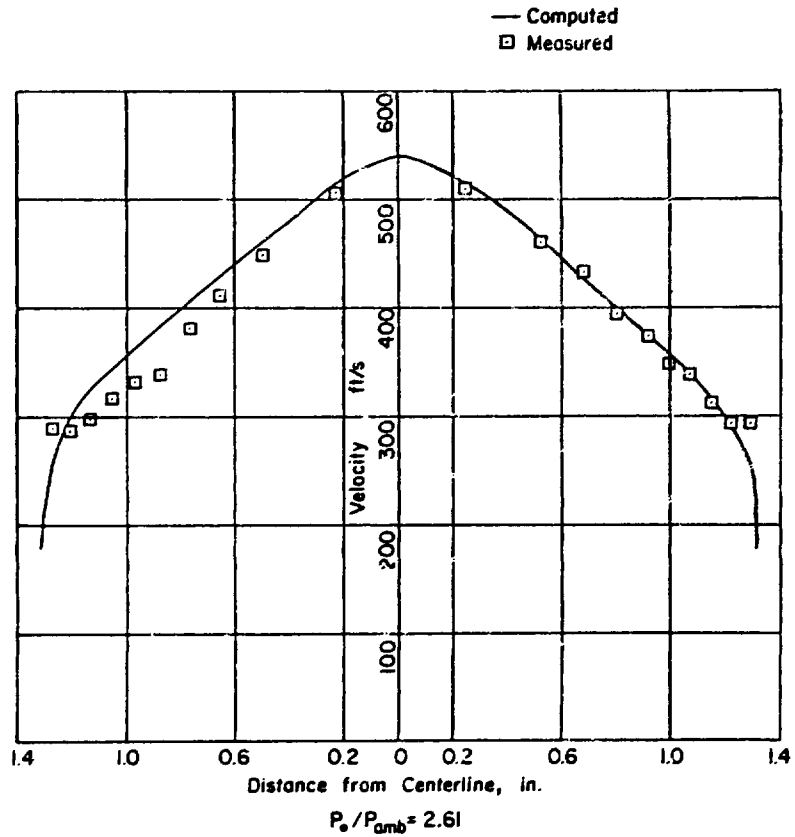

Figure 32. Typical velocity distributions at the mixing chamber exit, computed and measured. AR = 1.33, λ = 40.

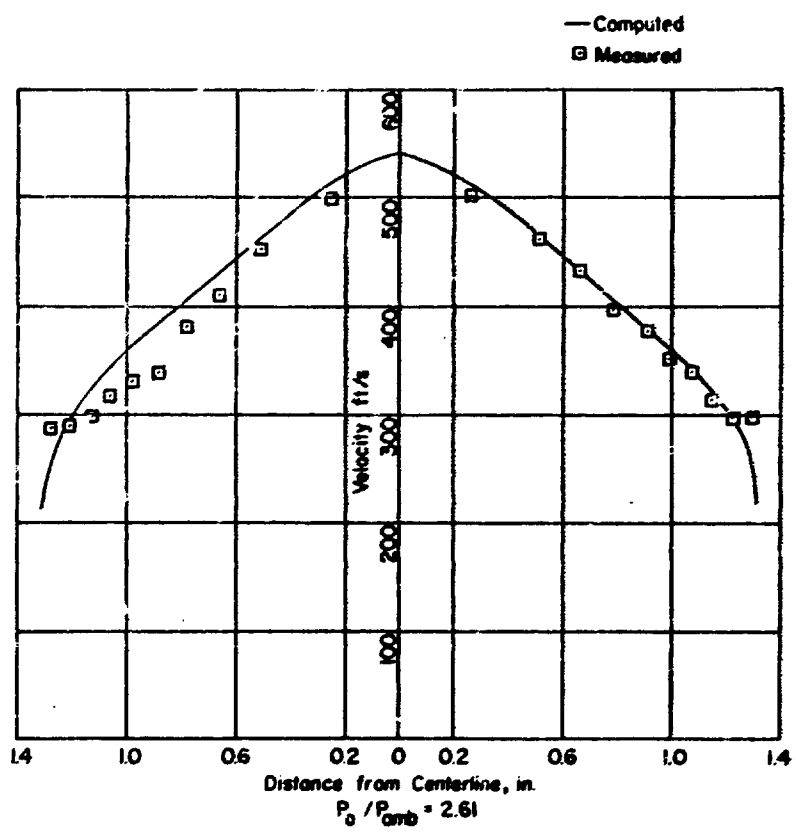

Figure 33. Typical velocity distributions at the mixing chamber exit, computed and measured. AR = 1.46, λ = 40.

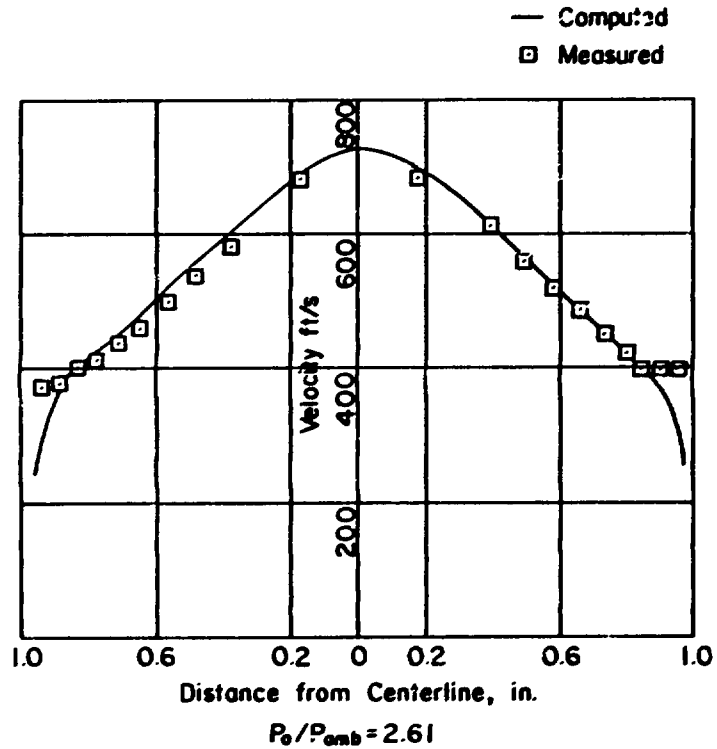

Figure 34. Typical velocity distributions at the mixing chamber exit, computed and measured. AR = 1.26, λ = 20.

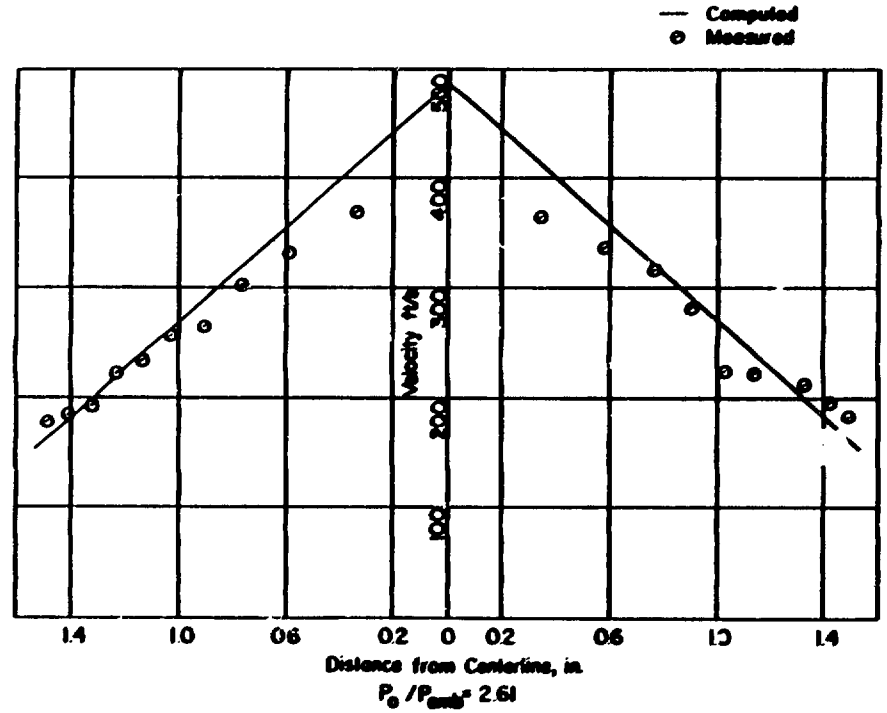

Figure 35. Typical velocity distributions at the diffuser exit, computed and measured. AR = 1.33, λ = 40.

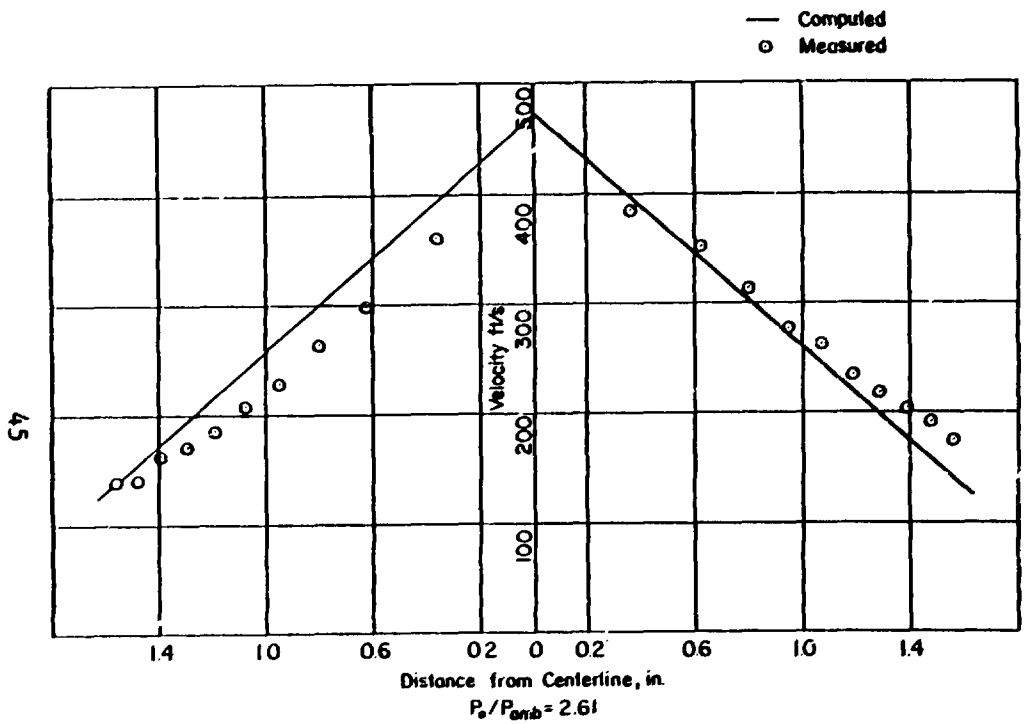

Figure 36. Typical velocity distributions at the diffuser exit, computed and measured. AR = 1.46, λ = 40.

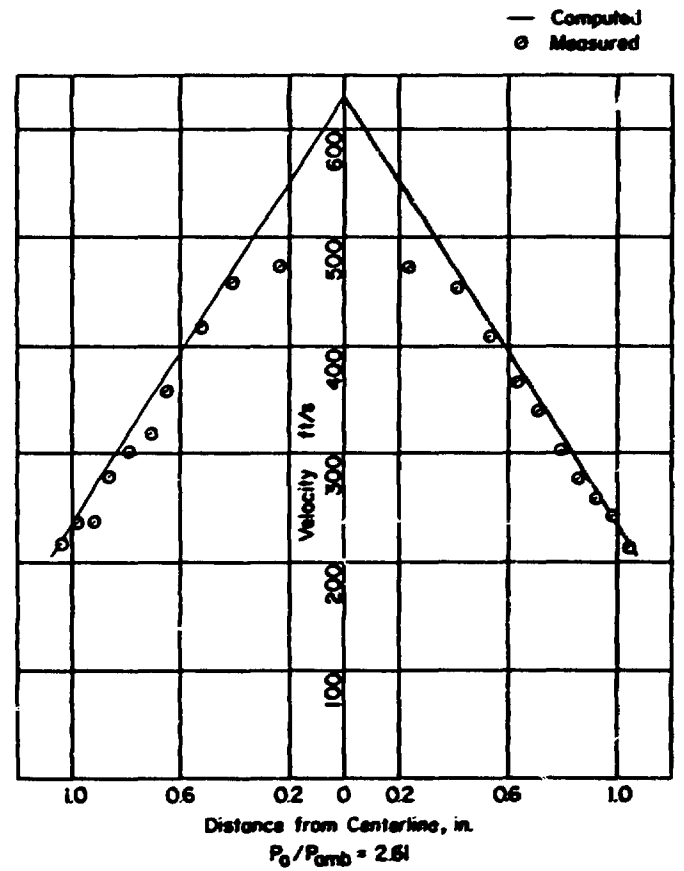

Figure 37. Typical velocity distribution at the diffuser exit, computed and measured. AR = 1.26, λ = 20.

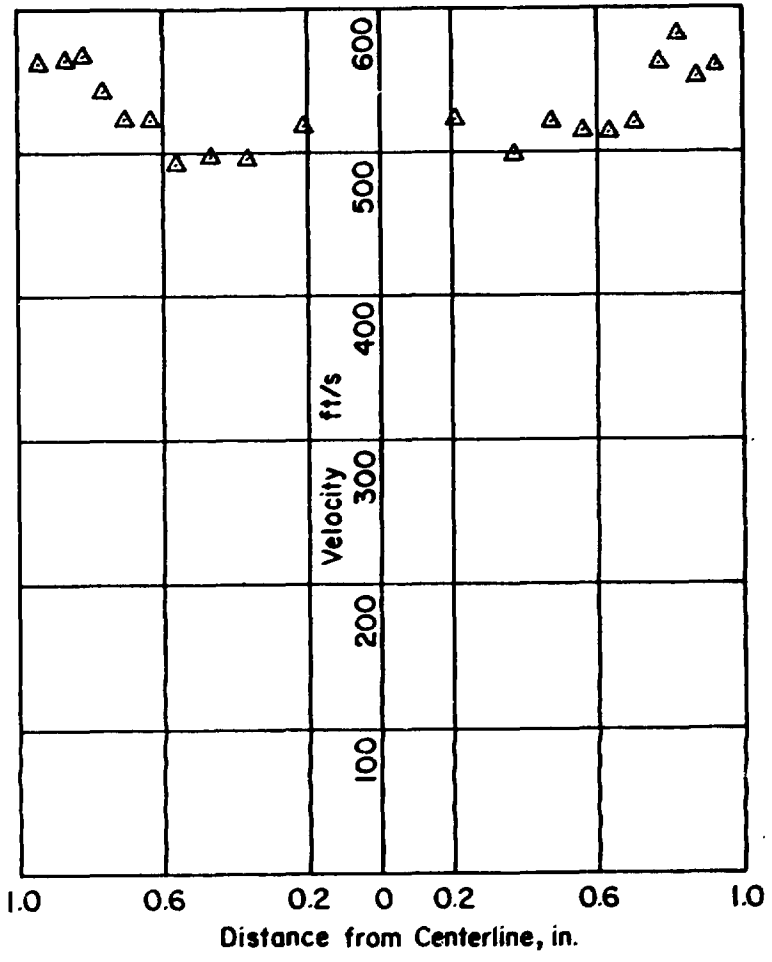

Figure 38. Unusual velocity distribution at the mixing chamber exit, measured. AR = 1.26, λ = 20.

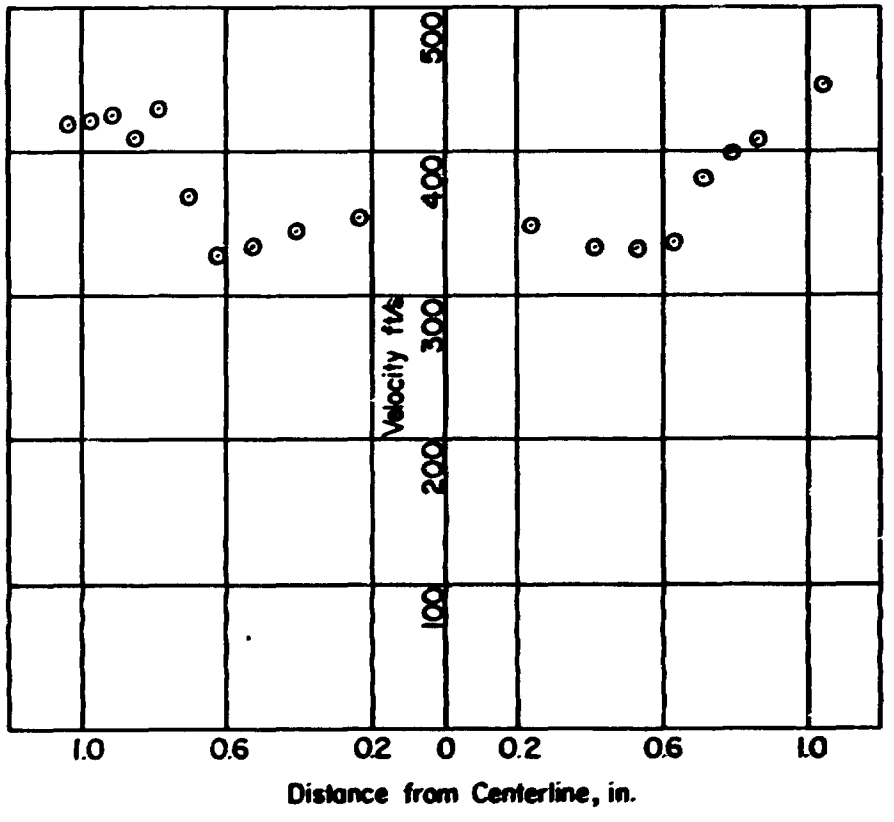

Figure 39. Unusual velocity distribution at the diffuser exit, measured. AR = 1.26, λ = 20.

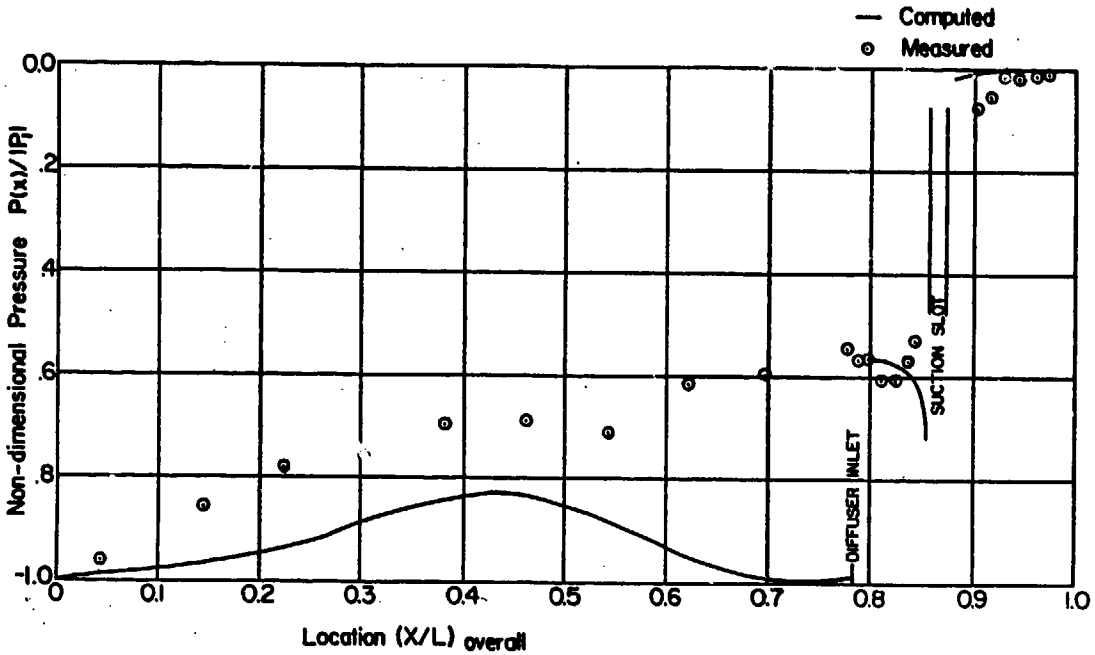

Figure 40. Comparison of mixing chamber and diffuser wall pressure distributions, measured and computed AR = 1.33, $\lambda = 40$.

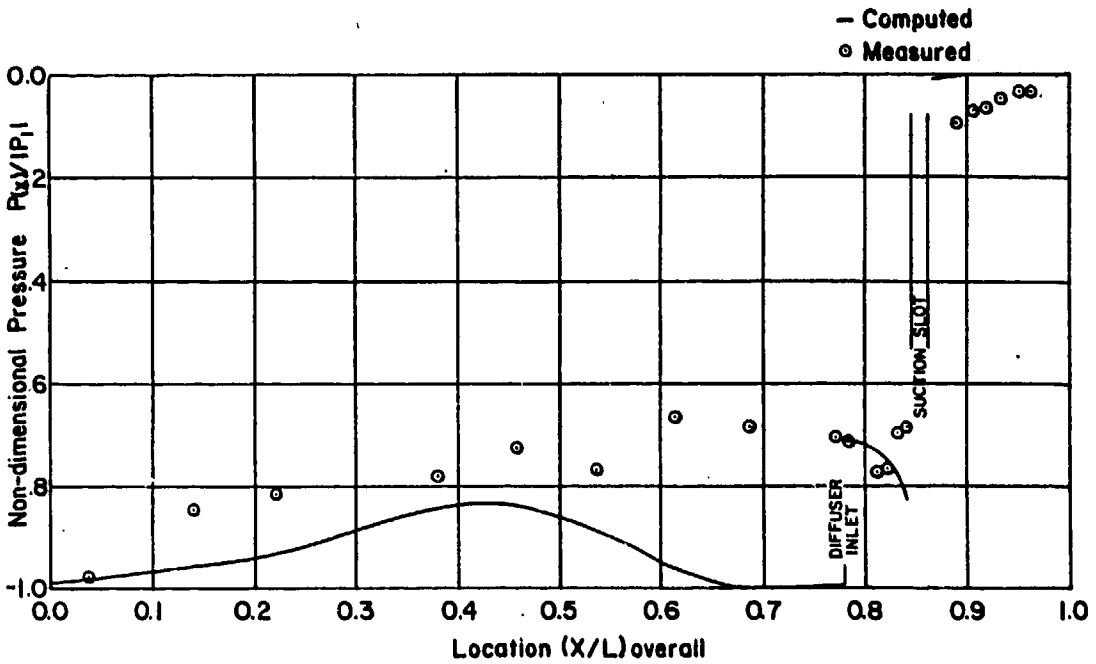

Figure 41. Comparison of mixing chamber and diffuser wall pressure distributions, measured and computed AR = 1.46, $\lambda = 40$.

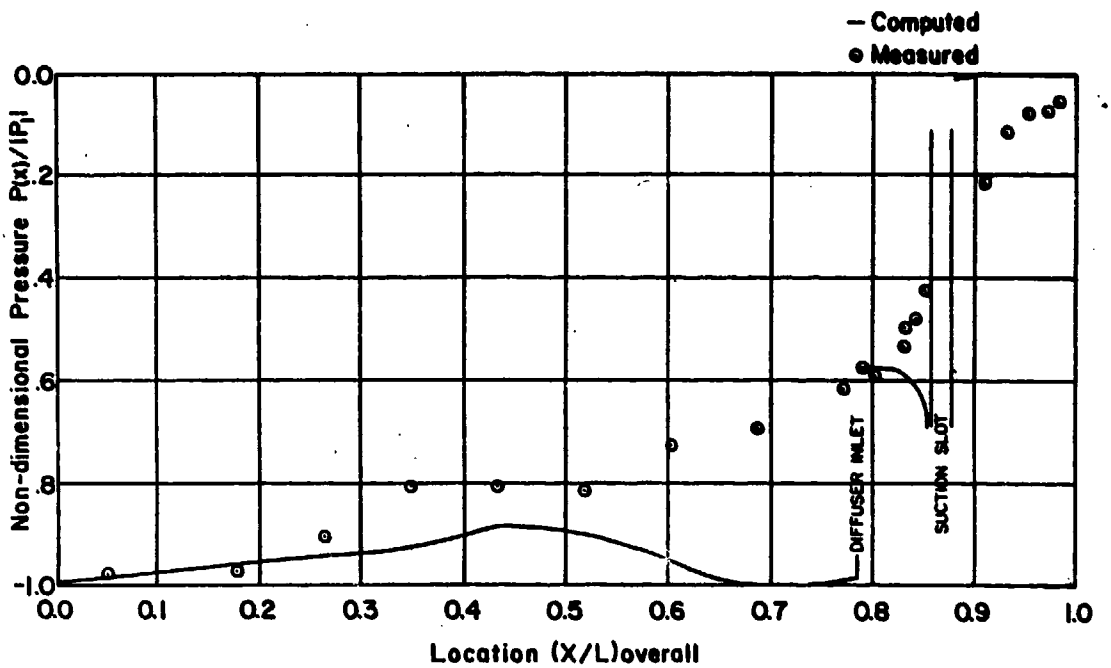

Figure 42. Comparison of mixing chamber and diffuser wall pressure distribution, measured and computed AR = 1.26, λ = 20.

APPENDIX A

A REFINED ROTATIONAL FLOW ANALYSIS

In view of the experimental difficulties encountered during the testing of an axisymmetric ejector designed (according to the theoretical considerations of Reference 1) for a mass ratio MR = 12 and with an inlet secondary to primary area ratio $\lambda = 40$, it became apparent that a modification of the diffuser analysis to account for the change of vorticity along the streamlines was necessary. In this analysis,[2] the governing equations of a rotational flow of constant vorticity at the inlet of a diffuser are derived. An auxiliary finite difference calculation is used to predict the flow behavior at the diffuser exit. In addition, the theoretical basis for a computer program analyzing a flow within a diffuser designed with potential flow theory and receiving a rotational flow of constant vorticity, is outlined

Governing Equations

The flow under consideration is assumed to be incompressible and axially symmetric. For the particular case of a Griffith diffuser designed with irrotational flow theory, it is further assumed that viscosity effects can be neglected if deceleration can be avoided along the diffuser wall. Under these circumstances, the governing equations for the fluid motion are:

1. Continuity:

For a cylindrical coordinate system in which x is the axial coordinate and r is the radial coordinate, the continuity equation is

$$\frac{\partial u_x}{\partial x} + \frac{\partial u_r}{\partial r} + \frac{u_r}{r} = 0 \qquad (1)$$

where u_x and u_r are the axial and radial components of velocity, respectively. Equation (1) leads to a stream function ψ defined by

$$u_x = \frac{1}{r}\frac{\partial \psi}{\partial r} \quad \text{and} \quad u_r = -\frac{1}{r}\frac{\partial \psi}{\partial x} \qquad (2a,b)$$

2. Vorticity:

The vorticity vector ω is defined by

$$\vec{\omega} = \vec{\nabla} \times \vec{u} \tag{3}$$

where $\vec{u}$ is the velocity vector. In the case of an axisymmetric nonswirl flow, the tangential component of $\vec{u}$ is zero, and no derivatives are considered in the tangential direction. Therefore, Equation (3) reduces to

$$\omega = \frac{\partial u_r}{\partial x} - \frac{\partial u_x}{\partial r} \tag{4}$$

Notice that the right side of Equation (4) is just the tangential component of $\vec{\omega}$, and the vector notation can be dropped. Substitution of (2,a) and (2,b) into (4) yields

$$\frac{\partial^2 \psi}{\partial x^2} + \frac{\partial^2 \psi}{\partial r^2} - \frac{1}{r}\frac{\partial \psi}{\partial r} = -\omega r \tag{5}$$

Equation (5) is the equation of motion to be solved. At the diffuser inlet ω is constant and known ($\omega = \omega_i$ at inlet); it varies along a streamline, and is therefore unknown in most parts of the diffuser. Figure A1 shows a fluid element of area A contained in a meridian plane. That element of area moves with the

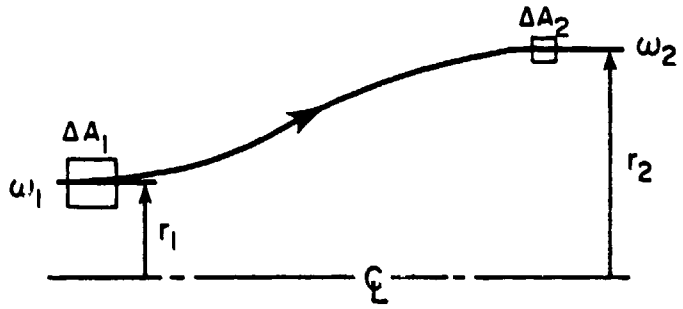

Figure A1. Fluid element at two positions.

flow, and the circulation around it is $\omega_1 \Delta A_1$. The circulation does not change when ΔA_2 reaches position 2, and therefore,

$$\omega_1 \Delta A_1 = \omega_2 \Delta A_2 \tag{6}$$

For an incompressible, axisymmetric flow,

$$r_1 \Delta A_1 = r_2 \Delta A_2 \tag{7}$$

or

$$\frac{\omega_1}{r_1} = \frac{\omega_2}{r_2} = \frac{\omega}{r} = \text{constant} \tag{8}$$

Equation (8) gives the relationship between the vorticity at an inlet point and values of vorticity at any downstream point on the same streamline.

Boundary Conditions

Solving Equation (5) requires knowledge of boundary conditions at the inlet, the exit, along the centerline, and along the walls of the diffuser.

1. Inlet: The flow at the inlet is assumed to be parallel. Therefore, u_r is zero and (2a) can be integrated to yield:

$$\psi = \frac{1}{2} u_x \ (x=0,\ r=0) \cdot r_i^2 - \frac{1}{3} \omega_i r_i^3 \tag{9}$$

where $u_x(x=0, r=0)$ is the centerline velocity at the inlet, and r_i is any radius at the inlet. ω_i is the inlet value of vorticity, which is constant.

2. Centerline: An equation governing the changes in vorticity can be written as:

$$\frac{D\omega}{Dt} = \frac{u_r}{r} \omega \tag{10}$$

Symmetry considerations suggest that $u_r = 0$ at the centerline. Therefore, ω is a constant along the centerline and equal to $_i$. Also, ψ is zero there.

3. Along the upstream wall: From Equation (9), ψ can be calculated at each inlet location including the wall. Along the upstream wall (upstream of stagnation point of the suction slot), ψ is constant and equal to the inlet value. Also, ω can be calculated as:

$$\omega = \frac{\omega_i}{r_{w,i}} \cdot r \tag{11}$$

where $r_{w,i}$ is the inlet radius at the wall.

4. Along the downstream wall: If the fraction of suction f.s. is specified, then can be specified along the downstream wall as

$$\psi = \psi_{st} = \psi_{w,i} \ (1 - \text{f.s.}) \qquad (12)$$

where $\psi_{w,i}$ is obtained from (9). However, because the coordinates of streamlines other than those of the diffuser walls are not known, cannot be calculated in a straightforward manner. The following sections show how these ω's can be found, and how boundary conditions at the diffuser exit can be calculated.

Auxiliary Analysis to Calculate Exit Boundary Conditions:

With the knowledge of the inlet radius of the diffuser, its area ratio AR, and f.s., it is possible to predict the flow conditions at the diffuser exit, provided that the flow is parallel at the exit. The scheme in Figure A2 overcomes the difficulty resulting from the fact that the coordinates of the streamlines are not all known, and that is not constant at the exit (which makes Equations (8) and (11) inapplicable).

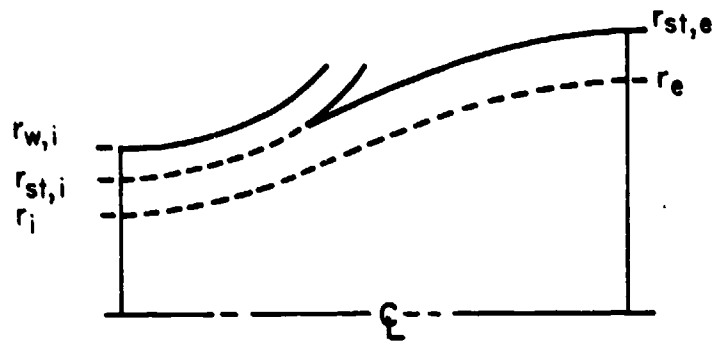

Figure A2. Exit boundary conditions.

Consider Figure A2, where selected streamlines along the diffuser are shown. Subscript "st" denotes conditions on the streamline corresponding to the stagnation point. From Equation (9), with $\psi = \psi_{st,e} = \psi_{st}$, $r_{st,i}$ can be calculated. Then $\omega_{st,e}$ is obtained as

$$\omega_{st,e} = \frac{\omega_i}{r_{st,i}} \ r_{st,e}$$

Now consider Equation (4) which for a parallel flow becomes:

$$\omega = - \frac{\partial u_x}{\partial r}$$

or in difference form

$$\Delta u_x = \omega \Delta r \tag{13}$$

If r is selected small enough, Equation (13) can be used to estimate $u_{x,e}$ (with an assumed $u_{x,w,e}$) as

$$u_{x,e} = u_{x,w,e} + \omega(r_{st} - r_e)$$

Now, Equation (2a) can be written in difference form as

$$\Delta \psi = r\, u_x\, \Delta r$$

which allows estimation of ψ_e as

$$\psi_e = \psi_{st,e} - (ru_x)_{ave}\,(r_{st,e} - r_e) \tag{14}$$

Equation (9), with $\psi = \psi_e$, can be used to solve for r_i, and ω_e can be calculated from

$$\omega_e = \frac{\omega_i}{r_i}\, r_e$$

Taking another step r at the exit, the above procedure is then repeated.

Equation (13) is used to calculate a new $u_{x,e}$, and Equation (14) is used to calculate a new ψ_e, etc. The calculation ends when $r_e = 0$. However, since $u_{x,w,e}$ was an assumed value, the values of $u_{x,e}$, ω_e, and ψ_e obtained at the end of the calculation are not necessarily correct. They are correct only for that particular value of $u_{x,w,e}$, which yields $\psi_e = 0$ at the centerline ($r_e = 0$). Therefore, an iterative procedure is necessary to obtain that value.

Flow Reversal in Inviscid Flow

One of the objectives of this analysis has been to explain some experimental observations suggesting the existence of a reverse flow in the diffuser near the wall when large values of vorticity are present at the diffuser inlet. In Figure A3, the results from the auxiliary analysis are presented. For an area ratio of 2.2 and an inlet nondimensional vorticity $\omega = 0.72$, the

analysis predicts a reverse flow near the wall, even though the flow is inviscid. The magnitude of the reverse flow increases as the suction rate increases, which is an undesirable situation. Table A1 gives $u_{w,e}$ obtained for various values of AR, ω_i and f.s. For the same area ratio the value of the velocity at the wall decreases when ω_i or f.s. increases. Also for the same and f.s., $u_{x,st,e}$ increases when AR decreases.

Overall Diffuser Analysis

As mentioned earlier, the above scheme only suffices to determine ψ along boundaries. But in order to solve Equation (5), it is necessary to know the values of ω in the entire diffuser. Since they are unknown, an iterative scheme was devised as follows:

1. Assume that is constant ($\omega = \omega_i$) in the diffuser, except along the boundaries where ω is known.
2. Solve Equation (5) with the known boundary conditions on ψ (boundary conditions at the slot exit are obtained the same way as those at the diffuser exit).
3. Knowing ψ at each point inside the diffuser, Equation 9 may be used to calculate r_i for each point (the inlet value of r corresponding to the value of ψ at that point). This ensures that the calculated inlet point is on the same streamline as the interior point. The vorticity at the interior point is then obtained by

$$\omega = \frac{\omega_i}{r_i} r$$

4. With the new values of ω, go back to step 2, the procedure is repeated until the difference between the old and new values of becomes suitably small.

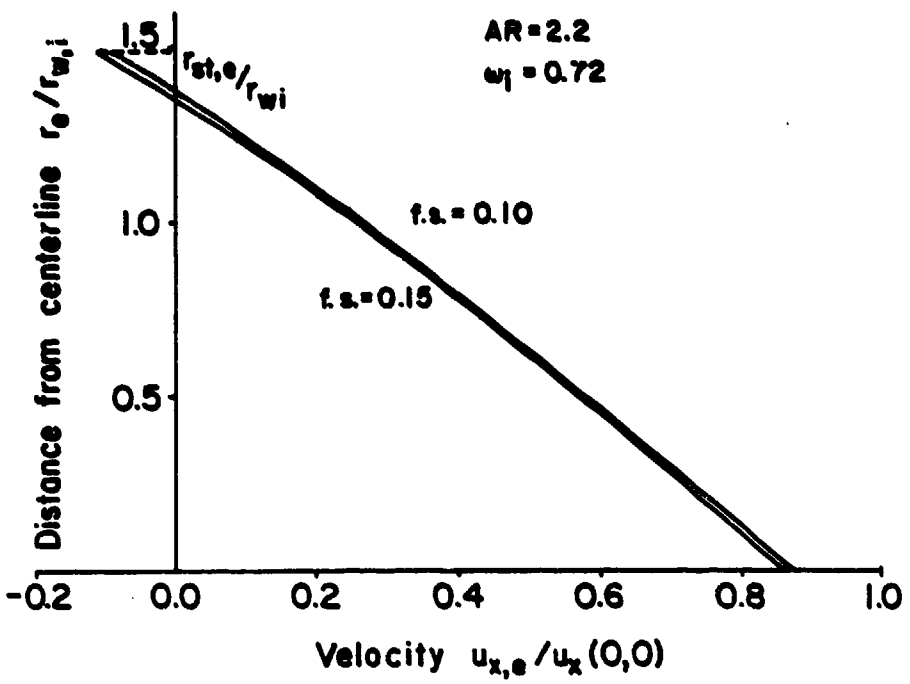

Figure A3. Velocity distirubtions at diffuser exit for AR = 2.2, ω = 0.72 at suction fraction of 10 and 15 percent.

Table A1. Results from short analysis for rotational flow.

AR	ω	f.s.	u
2.0	0.5	0.06	0.373
2.0	0.5	0.08	0.344
2.0	0.5	0.10	0.315
2.0	0.6	0.06	0.180
2.0	0.6	0.08	0.152
2.0	0.6	0.10	0.123
2.0	0.65	0.06	0.086
2.0	0.7	0.06	-0.006
2.2	0.5	0.06	0.221
2.2	0.5	0.08	0.194
2.2	0.5	0.10	0.167
2.2	0.525	0.06	0.171
2.2	0.525	0.08	0.145
2.2	0.55	0.06	0.124

APPENDIX B

METHOD OF DATA REDUCTION

The primary information sought in this investigation is the modified thrust augmentation ratio ϕ_2. This parameter is defined as:

$$\phi_2 = \frac{\sum_{i=1}^{n} (\dot{m}_i v_i)_e + \sum_{i=1}^{m} (\dot{m}_i v_i)_{e,aux}}{\dot{m}_p v_p + \dot{m}_{p'} v_{p'}}$$

where $\dot{m}_i$ and v_i are the mass flow rate and velocity at ith location. The subscripts e and e,aux stand for ejector exit and auxiliary ejector exit. The terms $\dot{m}_p$ and $\dot{m}_p'$ are the primary mass flow rates of the ejector and the auxiliary ejector, respectively. The velocities v_p and $v_{p'}$ are for the primary flows of the ejector and the auxiliary ejector, respectively.

The thrust augmentation ratio ϕ was calculated from the conventional definition as:

$$\phi = \frac{\sum_{i=1}^{n} (\dot{m}_i v_i)_e}{\dot{m}_p v_p}$$

The various parameters used in these equations were determined as follows:

1. The mass flow $\dot{m}_p$ was determined from turbine flow meter frequency, meter calibration constant and the density of air at the measured static pressure and temperature.
   The mass flow $\dot{m}_{p'}$ was determined from the pressure differential of the flow meter, meter calibration constant and the density of air at the measured static pressure and temperature.
2. For v_p, the Mach number of the flow at the exit of the converging nozzle was calculated from the ratio of the measured exit static pressure to plenum pressure (when this ratio is larger than the ratio for Mach number of one). Then the sonic speed was

determined from the static temperature of the air at the nozzle exit derived from the measured plenum temperature for an isentropic process. Finally, v_p was calculated from the Mach number and the speed of sound. When the pressure ratio is equal to or smaller than the ratio for flow to reach sonic speed, v_p was assumed to be the sonic speed. Similarly the $v_{p'}$ was determined.

3. For evaluating the term

$$\sum_{i=1}^{n} (\dot{m}_i v_i)_e$$

the ejector exit momentum and the exit mass flux $\dot{m}_e$ were determined from stagnation and static pressure measurements at 20 locations across the exit. From the ratio of the static to stagnation pressure, the local Mach number was determined. The exit static temperature was derived from the weighted stagnation temperatures of the primary and the secondary flows of the ejector, from which the local speed and density were determined. These 20 locations representing 10 equal areas (one circle and nine rings) were weighted equally to yield the total mass flux and momentum flux. For evaluating the term

$$\sum_{i=1}^{m} (\dot{m}_i v_i)_{e,aux}$$

the auxiliary ejector exit momentum and the mass flow rate $\dot{m}$ were determined in a similar manner except that the exit static pressure was assumed to be the ambient pressure, the total temperature was room temperature for both primary, and secondary flow, and 14 locations were used instead of 20 locations.

In addition to the above, other information regarding the operation of the ejector were computed. These are: the fraction of suction f.s. used in boundary layer control of the ejector diffuser, the entrained secondary flow $\dot{m}$ for ejector and $\dot{m}_{suc}$ for the auxiliary ejector, the mass ratios MR and $(MR)_{aux}$, the normalized static wall pressure distribution $P(x)/|P_1|$, and the thrust force on the mixing chamber.

4. The mass flow rate of the entrained flow of the auxiliary ejectors $\dot{m}_{suc}$ is the fluid removed from the diffuser for boundary layer control and was determined from the difference of $\dot{m}_{e,aux}$ and $\dot{m}_{p'}$. The $(MR)_{aux}$ was calculated from the formula

$$(MR)_{aux} = \frac{\dot{m}_{suc}}{\dot{m}_{p'}}$$

5. The entrained secondary flow $\dot{m}_{sl}$ was calculated using the formula

$$\dot{m}_{sl} = \dot{m}_e + \dot{m}_{suc} - \dot{m}_p$$

An alternative method was used for cross checking $\dot{m}_{sl}$ by traversing the exit of the mixing chamber. In this alternative method, $\dot{m}_{sl}$ was determined from the difference of the mass flow rate within the mixing chamber $\dot{m}_{mc}$ and the ejector primary mass flow ratio $\dot{m}_p$ or

$$\dot{m}_{sl} = \dot{m}_{mc} - \dot{m}_p$$

The method of computing $\dot{m}_{mc}$ is similar to that used for $\dot{m}_e$.

6. The MR, mass ratio of the ejector, was computed as:

$$MR = \frac{\dot{m}_{sl}}{\dot{m}_p}$$

The suction fraction for boundary layer control was computed from

$$f.s. = \frac{\dot{m}_{suc}}{\dot{m}_p + \dot{m}_{sl}}$$

7. The normalized wall static pressure distribution, $P(x)/|P_1|$, was used in preliminary testing to scrutinize the possible adverse pressure gradient. The first pressure tap is located immediately downstream of the bell mouth inlet, and its gage pressure reading was used as normalization factor.

8. The normalized velocity distribution at the mixing chamber exit was used to determine the vorticity at the diffuser inlet. Its centerline velocity and the radius of the diffuser at the inlet were used as normalization factors for velocity and linear distance.
9. The thrust force on the mixing chamber was obtained from a static load calibration curve and the strain gage reading. A computer thrust force F_{mc} based on exit momentum was determined from the formula

$$F_{mc} + (\phi-1)\ \dot{m}_p v_p$$

or

$$F_{mc} = (\phi-1)(\dot{m}v)_j \qquad \text{(Table 1)}$$

References

1. Yang, T., and El-Nasher, A. M., "Ejector Performance with a Short Diffuser," Proceedings of the Symposium on Jet Pumps and Ejectors, The British Hydromechanism Research Association, England (November, 1972).
2. Tripathi, B. N., "Ejector Performance with Short Axisymmeteric Diffuser," M. S. Project Report, Mechanical Engineering Department, Clemson University (May, 1983).
3. Yang, T., and Ntone, F., "Analytical Investigation of High Performance, Short Thrust Augmenting Ejectors," Mechanical Engineering Department, Clemson University, DTNSRDC-ASED-CR-1-82 (January, 1982).
4. Tai, T. C., "Optimization of Asixymmetric Thrust Augmenting Ejectors", AIAA Paper 77-707, presented at AIAA 10th Fluid and Plasmadynamics Conference, Albuquerque, NM, (June, 1977).
5. Yang, Tah-teh, and Nelson, C. D., "Griffith Diffusers," Journal of Fluids Engineering (December, 1979).
6. Nelson, C. D., and Yang, T., "Inverse Problem Design Method for Branched and Unbranched Axially Symmetric Ducts," AIAA Journal (September, 1977).
7. Ntone, F., "Method of Rotational Flow Calculations in a Griffith Diffuser," M. S. Thesis, Mechanical Engineering Department, Clemson University (1981).